Modelling and design of a flat plate fixed film photoreactor for phenol degradation

By

Francisco O. Galnares de la Garza

SET3811
System Integration Project II

Master of Science
in Sustainable Energy Technology

Student number: 4516796

Supervisor: Dr. Ir. Ruud van Ommen

Delft University of Technology

July 17, 2016

Table of Contents

Abstract 3
1. Introduction: The water problem 4
2. Photocatalysis 6
2.1. Photocatalytic mechanism 6
2.2. Photoreactors: types, challenges, and limitations 10
2.3. Photocatalytic water decontamination: Influence of physical parameters 12
2.4. Photocatalytic degradation of phenol 13
3. Photoreactor modelling 14
3.1. Radiation balance 15
3.2. Photocatalyst modelling 17
3.3. Fluid dynamic model and material balance along the reactor 18
3.4. Numerical solution 20
4. Results and Discussion 21
4.1. Radiation field and photocatalyst modelling 21
4.2. Photoreactor dimensions 23
5. Conclusions 26
Acknowledgments 27
Notation 28
Bibliography 29
Appendix A: Radiation model 34
Appendix B: Photoreactor length: steady state 35
Appendix C: Photocatalyst modelling 44

Abstract

This paper presents the mathematical modelling and design of a flat plate photoreactor with a fixed film photocatalyst to degrade phenol. Phenol was used as target pollutant as it is one of the most studied contaminants in photocatalysis and it is present in many of the wastewater streams containing pesticides, drugs, and dyes which cannot be treated with conventional wastewater technologies.

To model the photoreactor, first a Zero Reflectance Model assuming no energy absorption or scattering by the fluid phase was used to compute the rate of photon absorption. Interest was also placed on determining the effect of the photocatalytic film thickness on both the internal diffusion and the rate of photon absorption. Afterward, the material balance of the pollutant was computed considering convection, diffusion, and a Langmuir Hinshelwood type of kinetics to describe the degradation of phenol.

As the reaction just takes place at the bottom of the reactor, external mass transfer limited the overall phenol degradation. Therefore, several reactor heights were investigated to diminish external mass transfer limitations and determine the optimal photoreactor dimensions. For instance, for a throughput of 50 liters per day and assuming 10 hours of sunlight, to reach 95% phenol conversion the photoreactor height should be below 0.45cm, which corresponds to a photoreactor length of approximately 25 meters. In contrast, when the reactor height was diminished to 0.1cm, the required reactor length to reach 95% conversion decreased to 10 meters.

Keywords: advanced oxidation technologies, heterogeneous catalysis, photocatalysis, titanium dioxide, mineralization, fixed film, flat plate photoreactor, phenol, photocatalyst thickness, Langmuir-Hinshelwood, diffusion, diffusion limitation, local rate of photon absorption, conversion, residence time.

1. Introduction: The water problem

Inadequate access to clean drinking water and sanitation has become one of the most common problems affecting people all around the world. In 2010, the United Nations declared the access to clean drinking water a human right [1] and how a more sustainable water management is critical to achieve the Millennium Development Goals [2]. However, due to industrial development, global population growth, and long-term droughts caused by climate change, the number of people without access to clean drinking water is just expected to increase [3].

According to Malato et al [4], it is estimated that around 4 billion people worldwide have little or no access to clean or sanitized water supply. Although the lack of access to clean drinking water and sanitation pose a global challenge, the problem is worse for developing countries where water resources are limited and about half of the population suffers from one of the main waterborne diseases caused by microbial and viral pathogens (such as diarrhea), worm infestation (such as *Ascaris* and *Hookworm*), and bacteria (such as trachoma) [5].

In addition, emerging contaminants such as pharmaceuticals, personal care products, pesticides, drugs, dyes, and endocrine-disruptive compounds have been found in treated wastewater, surface waters, and drinking water [6,7]. These emerging contaminants cannot be treated with conventional wastewater technologies [8] and may accumulate in the aquatic environment where they cause interferences with the endocrine system of higher organisms, and microbiological resistance in soil, plants, and animals [9].

For instance, conventional filtration technologies remove the pollutants from the liquid phase by concentrating them in the retentate, which creates a secondary pollution problem as the retentate requires further treatment [10]. Additionally, reverse osmosis, membrane filtration, and adsorption with activated carbon involve high energy consumption and high operating costs [11].

Advanced biological treatments are only effective on biodegradable compounds that can be attacked by the specific microbial system [12]. Chemical processes such as chlorination or ozonation are unable to mineralize all organic pollutants; and due to their high operating costs [13], they are only economically viable when the pollutants are present in high concentrations [14]. When using chlorination, certain disinfecting byproducts (DBPs) known as potential carcinogens such as trihalomethanes are formed [15]. On the other hand, ozonation avoids most of the hazardous DBPs associated with chlorination processes, but small amounts of bromate ions are still generated [16].

The inadequate removal of emerging contaminant by conventional water treatment technologies has led to the rapid development in Advanced Oxidation Technologies (AOTs). These AOTs are based on the generation of high reactive species (OH, $O_2^{\bullet-}$, O_3) capable of completely degrading organic compounds, water pathogens, and

disinfect byproducts [4,17]. Among these AOTs, photocatalysis has been proposed as a viable and highly efficient process to degrade organic compounds and mineralize them into carbon dioxide and water [3]. However, unlike other AOTs which are based on the use of additional chemical reactants, the kinetic behaviour of photocatalysis usually follows a saturation behaviour [18]; which is why typical applications of photocatalysis are at a low concentration of pollutants.

2. Photocatalysis

Photocatalysis is an attractive technology because of its various potential applications in disciplines such as selective chemical synthesis [16], environmental technology [18], and medicine [19]. Although heterogeneous catalysis in selective processes is not frequently employed, there is increasing interest in those processes due to its possibility to avoid heavy metal catalysts, strong chemical oxidants or reducing agents, and high operating temperature and pressure [20]. Selective photocatalytic applications include organic transformations for the synthesis of fine chemicals such as the reduction of carbon dioxide into methanol [20–24], water splitting for hydrogen production [16,18,20], and selective oxidation of organic compounds such as alcohols to carbonyls [16].

Regarding medical applications, cancer treatment is one of the most important applications associated with photocatalysis [19]. For example, a 30-minute illumination in the presence of TiO_2 leads to complete killing of human U 937 monocytic leukemia cells [25]. However, as the skin presents weak penetration of UV light, the use of fiber optics or surgery is usually needed for this application [26]. Other medical applications of photocatalysis include photokilling of pathogenic microorganisms, bacteria, and viruses in environments where biological contamination must be prevented [27].

Non-selective applications are mainly applied to environmental remediation of non-biodegradable molecules from water and air [18]. Here, the contaminants are mineralized into stable inorganic molecules such as carbon dioxide, water, and salts. In environmental technology, photocatalysis has also been employed to disinfect wastewater streams [16]. Even though inactivation of bacteria via photocatalysis is currently restricted to low volumes of water with low microbial contamination [28] it has proven to kill efficiently very resistant Gram-negative bacteria, such as *Enterobacter cloacae* which can otherwise not be inactivated [29].

2.1. Photocatalytic mechanism

The overall heterogeneous photocatalytic process follows the same steps as conventional heterogeneous catalysis [21]. As it is illustrated in Figure 1, the reactants first have to diffuse from the fluid phase to the surface of the catalyst where they are adsorbed. Once adsorbed, they react on the surface of the catalyst. Afterward, the products are desorbed from the catalyst surface and diffuse onto the fluid phase.

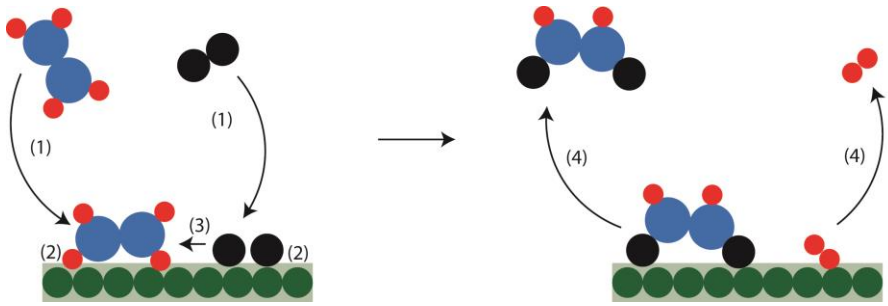

Figure 1: Schematic representation of the main steps in heterogeneous catalysis: (1) transfer of reactants from the fluid phase to the surface of the catalyst; (2) adsorption of the reactants on the surface of the catalyst; (3) reaction in the adsorbed phase; (4) desorption of the products into the fluid phase (after [30]**).**

The main difference with conventional catalysis is that photo-induced reactions are activated by the absorption of a photon rather than by thermal energy [21]. When a semiconductor catalyst is illuminated with photons with equal or greater energy than the band gap of the catalyst, these photons are absorbed and an electron-hole ($e^- h^+$) pair is generated. Although thermal energy is inadequate to activate the photocatalyst, the temperature of operation is still an important parameter [3]. Operating at low temperatures favours adsorption; hence, the desorption of the products will limit the reaction rate. On the opposite, operating at high temperature limits the adsorption of the reactants onto the TiO_2 surface and promotes the recombination of charge carriers. As a consequence, the optimum operating temperature has been found between 20°C and 80°C [21].

Various semiconductor catalysts such as ZnO, ZrO_2, TiO_2, CeO_2, CdS, Fe_2O_3 have been investigated for photocatalytic processes [21]. Nonetheless, the best photocatalytic performances are always obtained with TiO_2 [13,31–35]. Titanium dioxide is the most active photocatalyst under the photon energy of 300 to 390nm [3] and has the advantages of being chemically and biologically inert, photocatalytically stable, cheap, easy and safe to manufacture and use, and it is able to efficiently catalyse reactions [21,31]. Figure 2 illustrates some of the aforementioned catalysts together with the redox potential of some organic compounds.

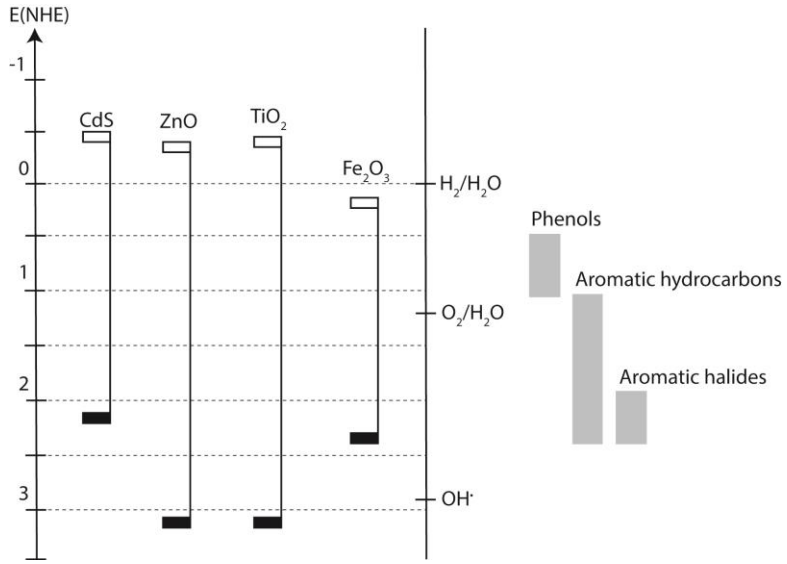

Figure 2: Band positions (top = valence band, bottom = conduction band) of several semiconductors together with the redox potential of some organic compounds (after [16]**).**

Despite all the aforestated advantages of TiO_2, its bandgap of 3.0 (for rutile) or 3.2 eV (for anatase), means that it is only activated by ultraviolet (UV) light and not by visible light [3]. As only 5% of the sunlight reaching the Earth's surface is in the near UV wavelength, one of the most active areas of research is that of doping the catalyst to shift its activating wavelength to the visible spectrum as the efficient use of solar light will decrease costs considerably [24].

Figure 3 presents a schematic of the photocatalytic process with TiO_2 as photocatalyst when it is excited with adequate photon energy ($h\nu$), together with some of the redox reactions that take place [3,18,24]. As the photon is absorbed, the electron (e^-) is promoted from the valence band to the conduction band (e^-_{CB}), generating a hole in

the valence band (h^{+}_{VB}) (see also Equation (2.1)). Generally, during the transport of the photogenerated electrons and holes to the catalyst surface, two things can happen: they either recombine and dissipate energy as heat (see also Equation (2.4)), or they react with an electron acceptor and an electron donor on the particle surface, and initiate the reduction and oxidation processes, respectively [21,22,24].

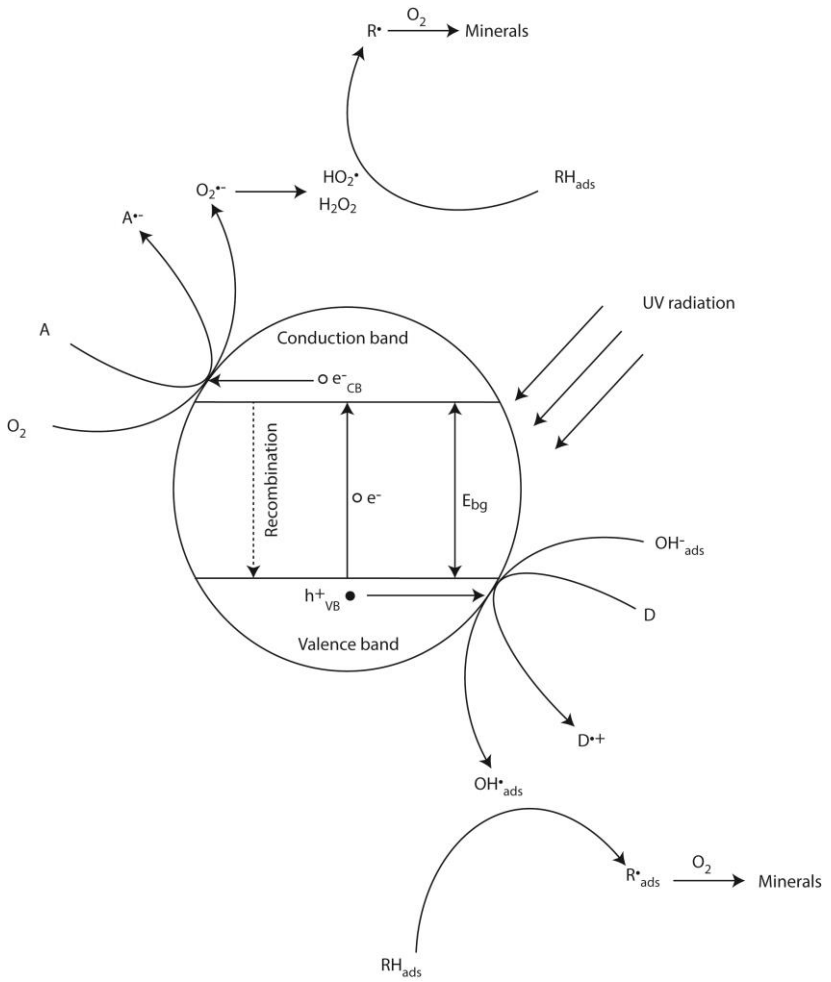

Figure 3: Schematic mechanism of electron-hole pair formation of a spherical TiO_2 particle together with some of the redox reactions that take place (after [18]**).**

The photogenerated electron that reached the surface of the catalyst (e^{-}_{TR}) must react to avoid recombination. Therefore, electron acceptors (or scavengers) must be present [18]. Oxygen is the most commonly used electron acceptor. The oxygen-involved species ($HO_2^{\cdot}$, HO_2^{-}, O_2, $O_2^{\cdot-}$, H_2O_2) are present either in the interface or in the bulk solution and participate in the degradation kinetics which leads to the final mineralization of the organic species [18,36].

After the photogenerated hole diffuses towards the surface of the catalyst (h^{+}_{TR}), it either reacts with the adsorbed solvent molecules (see also Equation (2.6)), or with an adsorbed substrate by interfacial electron transfer, oxidizing the adsorbed species (see also Equation (2.7)) [18,36,37]. It should be noted that the hydroxyl radicals with an unpaired electron are highly reactive species, which due to their high oxidation potential of 2.80V are capable of oxidizing almost all organic pollutants in water [18].

Photoexcitation: $TiO_2 + h\nu \rightarrow h^+_{VB} + e^-_{CB}$ (2.1)

Charge carrier trapping: $e^-_{CB} \rightarrow e^-_{TR}$ (2.2)

Charge carrier trapping: $h^+_{VB} \rightarrow h^+_{TR}$ (2.3)

Electron-hole recombination: $e^-_{CB} + h^+_{VB} \rightarrow heat$ (2.4)

Reduction: $e^-_{TR} + O_{2,ads} \rightarrow O^{\bullet -}_{2,ads}$ (2.5)

Oxidation: $h^+_{TR} + OH^-_{ads} \rightarrow OH^{\bullet}_{ads}$ (2.6)

$h^+_{TR} + RX_{ads} \rightarrow RX^{\bullet +}_{ads}$ (2.7)

According to Turchi and Ollis [38], once the hydroxyl radical is formed, the reaction can take place in four different situations:

i. The reaction occurs while both species are adsorbed

$OH^{\bullet}_{ads} + R_{1,ads} \rightarrow R^{\bullet}_{2,\text{ads}}$ (2.8)

ii. A non-bound radical reacts with an adsorbed organic species

$OH^{\bullet} + R_{1,ads} \rightarrow R^{\bullet}_{2,\text{ads}}$ (2.9)

iii. An adsorbed radical reacts with a free organic species that diffuses towards the catalyst surface

$OH^{\bullet}_{ads} + R_1 \rightarrow R^{\bullet}_2$ (2.10)

iv. The reaction happens between two free species in the bulk solution

$OH^{\bullet} + R_1 \rightarrow R^{\bullet}_2$ (2.11)

Although all the aforementioned situations are possible, the main photocatalytic degradation process takes place on the surface of the catalyst (Equations (2.8) to (2.10)) [18].

Moreover, the electron-hole recombination must be prevented as much as possible. As mentioned before, recombination corresponds to the degradation of photoenergy into heat; hence, reducing the quantum yield [21]. Strategies to diminish the electron-hole recombination include doping [39], surface modification of the catalyst [40] and amalgamation with electron scavenging agents [41]. The latter one has been the most popular approach where scavenging agents such as metals [42], carbonaceous materials [43], and polymers [44] have been investigated. Although under the carbonaceous materials carbon nanotubes, fullerenes, and graphene have been investigated, graphene has had the greatest interest due to its ease of fabrication [35], its large surface area (2600 m^2g^{-1}) [45], optical transparency [46], excellent mechanical strength [47], high thermal conductivity [48], and high room temperature charge carrier mobility [49].

Graphene also plays a major role in water decontamination as the formation of a π-π stacking between the aromatic rings of graphene and organic pollutants facilitates their adsorption and thus enhances its quenching [20,35]. However, for an efficient synergistic effect catalyst-graphene, the amount of metal oxide loading to the graphene support has to be optimized. Graphene improves the photocatalytic activity of the catalyst until a certain threshold. Beyond that threshold limit, reduction of the photocatalytic activity occurs due to the absorption and scattering of photons by excess carbon content [35]. Despite all the advances in graphene technology, still further research is needed to fully understand the interactions between graphene and metal oxides to design more effective photocatalysts.

2.2. Photoreactors: types, challenges, and limitations

The design of a photoreactor differs from traditional chemical reactors as the geometry of the reactor is of significant importance to guarantee that photons are collected in an effective way by the photocatalyst. Several reactors have been proposed for photocatalytic processes: slurry reactors, annular reactors, immersion reactors, optical tube reactors, optical fiber reactors, among others [24]. Nonetheless, industrial applications have remained limited, mainly for two reasons:

i. Photon transfer limitations
ii. Mass transfer limitations

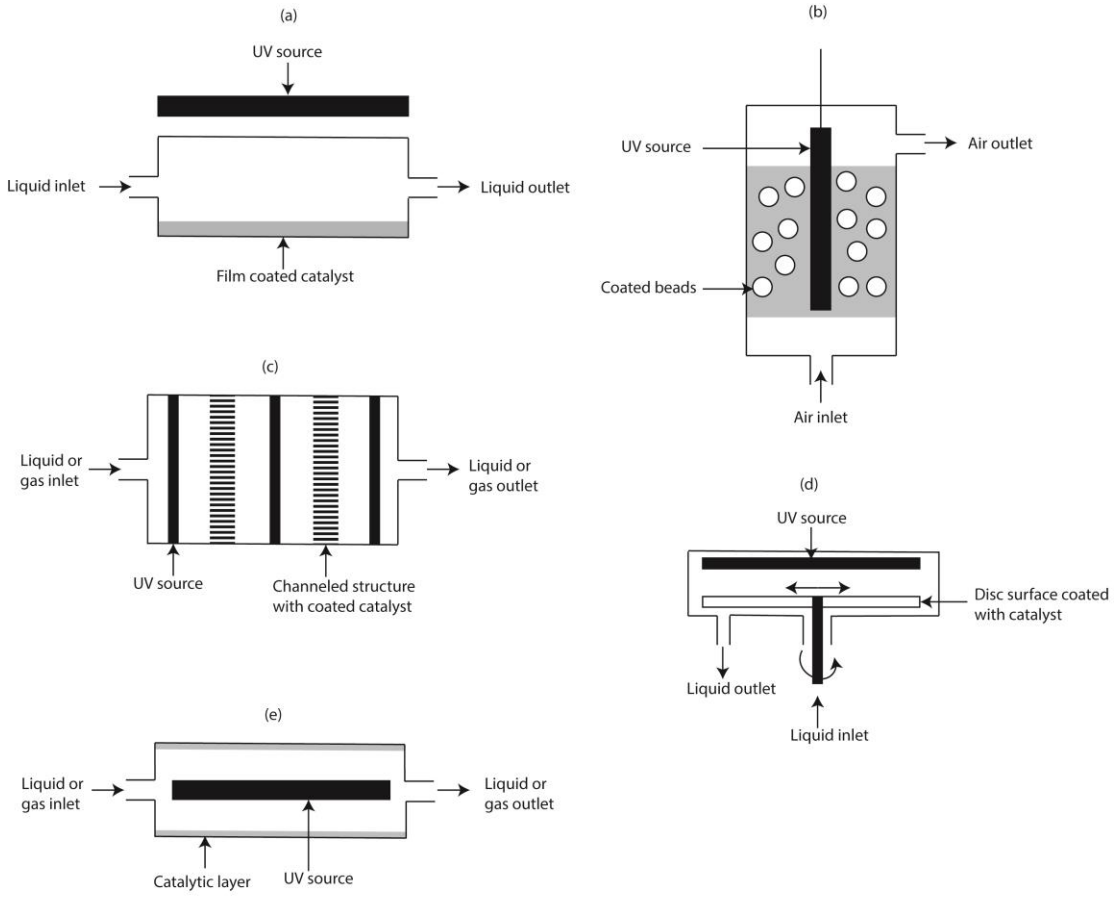

Figure 4: Examples of different photoreactors: (a) Flat-plate with immobilized catalyst photoreactor (after [50]**), (b) Slurry fluidized bed photoreactor (after** [51]**), (c) Monolith photoreactor (after** [52]**), (d) Spinning disc photoreactor (after** [53]**), (e) Annular photoreactor (after** [54]**).**

With respect to photon transfer limitations, it has to be noted that the irradiance of light decreases inversely with the square of the distance from the source of light; hence, a small distance between the light source and the catalyst is preferred. In addition, light may be absorbed on the way to the catalyst as it has to travel through the fluid. Thus, it is very difficult to achieve uniform irradiance throughout the catalyst surface. Better uniformity may be achieved by increasing the distance between the light and the catalyst; however, this will decrease the average incident irradiance [24].

To overcome photon transfer limitations, optical fibers is the most investigated technology [24,55]. In optical fibers, light is propagated along their length by

reflection on the fiber and the catalyst is typically coated on the stripped fibers. However, the main drawbacks are that light intensity decreases exponentially along the axial direction of the fiber and that charge carriers are generated far from the liquid-catalyst interface, augmenting the probability of recombination. Still much research is needed to optimize certain parameters such as the thickness of the coating, the fiber diameter, and the fact that optical fibers may take up a large fraction of the reactor volume [24].

To avoid mass transfer limitations, the contact between the catalyst and reactants should be maximized. Slurry systems are by far the most investigated photoreactors [21,24,32] as there is good contact between the catalyst and the reactants. However, their main drawback is the catalyst recovery downstream, which increases operation costs [56]. Among slurry photoreactors, fluidised bed photocatalytic reactors (see Figure 4b) have been proposed to overcome mass transfer limitations. Even though they have the associated problems of being a dispersed phase reactor, the generation of bubbles enhances light penetration compared to conventional slurry reactors [24,32].

Another disadvantage of slurry systems relies upon that the penetration of the light is further limited by the absorption of the TiO_2 particles and dissolved organic species [57], which is why many other researchers advocate for reactor designs with immobilized catalysts over suitable supports. Among the immobilized bed reactors, spinning disc reactors (see Figure 4d), monolith reactors (see Figure 4c) and microreactors have been investigated.

Even though monolith reactors allow operating with high flow rates, low-pressure drops, and provide high surface-to-volume ratio, they present low light efficiency [52]. The use of microreactors for photocatalytic purposes is perhaps the most promising area of research to overcome both photon transfer and mass transfer limitations [58]. The use of microscale illumination provides both a large catalyst surface area per unit of reactor volume and high illumination efficiency; however, their relatively small throughput is the main drawback of microreactors.

Moreover, during the past years, flat-plate photocatalytic reactors (see Figure 4a) have been considered as efficient reactors to treat both polluted air and water quickly and efficiently [50,54,59,60]. Some of the advantages of these reactors are high surface-area-to-volume ratio, low pressure drop, relatively uniform distribution of light radiation, and flexible enough for large-scale applications [60].

Besides eliminating the need for the catalyst particle separation downstream, the use of immobilized catalysts provides at least two other important advantages compared to slurry reactors. Firstly, the catalyst film is porous, and thus provides a large surface area for the degradation of contaminant molecules [57]. Secondly, when a conductive material is used as a support, the catalyst film can be connected to an external potential to remove excited electrons and reduce electron-hole recombination [57,61]. Nevertheless, when the catalyst is immobilized, mass transfer limitations may arise. On the one hand, external mass transfer may limit the degradation rate at low fluid flow rate due to the increasing diffusional length of the reactant from the bulk solution to the catalyst surface. On the other hand, internal mass transfer limitations may be present with increasing catalyst film thickness. These properties of

immobilized catalysts usually lead to a lower overall degradation rate compared to slurry systems [62].

2.3. Photocatalytic water decontamination: Influence of physical parameters

To have a rapid photocatalytic reaction rate, several water quality parameters have to be ensured. If the water has high turbidity, the presence of such particles will affect the optical properties by scattering and absorbing light; thus, impeding the penetration of the UV light. According to Gelover [33], in photocatalytic water decontamination, the turbidity must be kept below 5 nephelometric turbidity units (NTU).

The presence of inorganic ions can also hamper the photoactivity of the catalyst. Overall, at a certain level, the presence of Cu^{2+}, Fe^{2+}, Al^{3+}, Cl^{-}, PO_4^{3-} may have negative effects on the photoreaction rate; whereas oxyanions such as ClO_2^{-}, ClO_3^{-}, IO_4^{-}, $S_2O_8^{-}$, and BrO_3^{-}, may increase the photoreaction rate by scavenging electrons and thus diminishing electron-hole recombination [63]. Because of this, water pretreatment with ion exchange resins is one of the few methods that is used to reduce inorganic ion disturbances in the photocatalytic activity.

In photocatalytic water treatment, pH is one of the most important operating parameters. Any change in the pH will affect the surface charge on the catalyst particles, the size of the catalyst aggregates, and the positions of the valence and conduction bands [3,64]. Researchers have usually used the point of zero charge (PZC) to study the effect pH has on the photodegradation kinetics. The PZC of TiO_2 is a condition where its surface charge is zero (pH=6.5) [64]. In this point, there is an absence of any electrostatic force, thus, the interaction between the photocatalyst and water contaminants is minimal. Different pH will affect the surface charge density according to the following water equilibrium equations:

pH<PZC: $TiOH + H^+ \rightleftharpoons TiOH_2^+$ (2.12)

pH>PZC: $TiOH + OH^- \rightleftharpoons TiO^- + H_2O$ (2.13)

When the pH is lower than the PZC (Equation (2.12)), the surface charge of the catalyst becomes positively charged and attracts the negatively charged compounds. On the other hand, when the pH is higher than the PZC (Equation (2.13)), the catalyst surface becomes negatively charged and will repulse anionic compounds in water [3,64].

Finally, dissolved oxygen also plays an important role in the photocatalytic degradation of water contaminants to ensure there are sufficient electron scavengers to avoid recombination [3]. According to a study made by Wang and Hong [65], low dissolved oxygen, although degrading the contaminant, will hamper its mineralization. Nonetheless, the effect of dissolved oxygen in photocatalytic reactions has received little attention and its effect on the TiO_2 surface photoactivity is not clearly known [3].

2.4. Photocatalytic degradation of phenol

In the last decade, extensive studies on the degradation and mineralization of organic contaminants have been performed (see for example the review papers: [38,66,67]. Special interest has specifically been placed to study the degradation of aromatic compounds, including phenol and its derivatives. Usually, the full mineralization of aromatic compounds on the surface of titania, proceeds via many steps [68]. Even though the determination of the intermediate compounds has been subject of many investigations [69–71], a full mechanism has not yet been established [68]. As an example, Figure 5 illustrates a possible mechanism for the photomineralization of phenol. Here, phenol is hydroxylated by the $OH^{\bullet}$ radicals, which leads to successive oxidation/addition until the ring opens. Once the ring is opened, the intermediates, which are mostly aldehydes and carboxylic acids are further carboxylated to carbon dioxide and water [3].

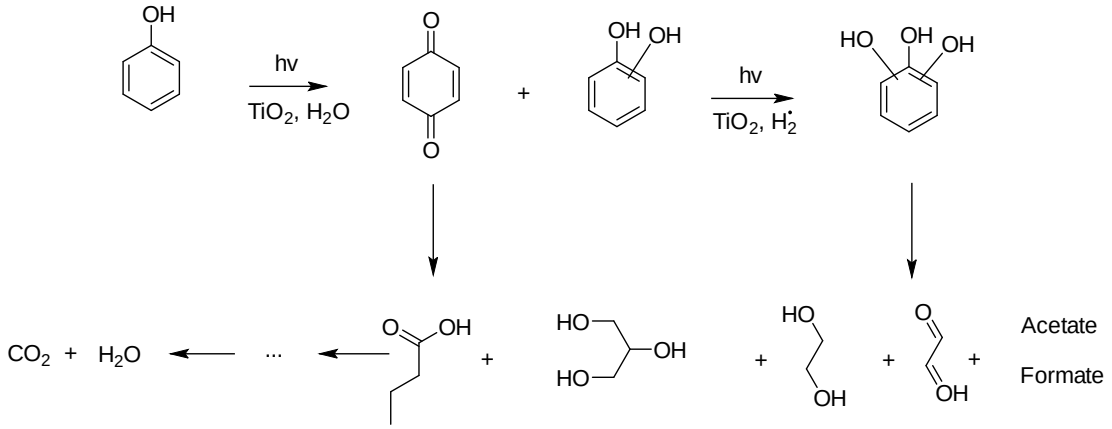

Figure 5: Possible mechanism of phenol mineralization on TiO_2 photocatalyst (after [68]**).**

3. Photoreactor modelling

Photoreactors can be considered "four phases" systems, where gas, liquid, solid, and light are strongly coupled [56]. As a consequence, to efficiently design a photoreactor, it is necessary to model the interaction between the catalyst, pollutants, and radiation, which makes the optimization of photocatalytic processes very complex [72]. The thickness of the catalyst, together with other factors such as porosity, total surface area, and light absorption influence the final pollutant conversion and as a consequence the overall efficiency of the system [73].

It is important to note that depending on the type of reactor used, being slurry or fixed bed, the modelling of the system follows a different approach [74]. In slurry reactors, the coupling between mass balance and light is very strong as the dispersed photocatalyst particles have strong absorbance and scattering effects which influence the light distribution inside the reactor. Thus, the models used usually focus more on the light absorption in the reactor whereas the fluid dynamics are usually simplified assuming a perfectly mixed reactor [75].

In contrast, in a reactor with immobilized catalyst, the coupling between mass and light is less strong as the photocatalyst is deposited as a film and its position never changes with respect to the light. Thus, to model these systems, the light model is usually simplified and more attention is paid to internal and external mass transfer phenomena, which are critical issues in fixed film reactors. External mass transfer limitation is typical in flat plate reactors where the flow is poorly mixed due to its laminar regime and the pollutant has to travel through many layers of fluid to reach the active photocatalyst surface. Internal mass transfer is a phenomenon that occurs in porous media and involves the diffusion of a molecule from the external surface of the catalyst to the inside of the pore; hence, this phenomenon is of crucial importance in the evaluation of the optimal film thickness for porous catalysts [74,75].

A simplified schematic representation of the radiation and pollutant concentration profiles in a flat plate fixed film photoreactor where the catalyst is illuminated from the liquid-solid interface is shown in Figure 6.

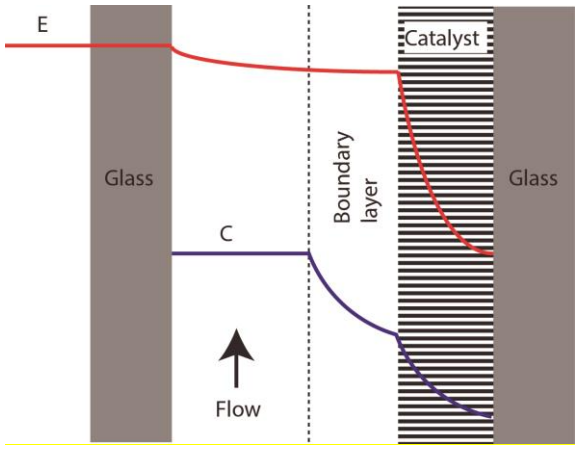

Figure 6: Schematic representation of the radiation and pollutant concentration profile in the flat-plate photocatalytic reactor considering external mass transfer limitations and light absorption by the flow (after [72]**) .**

3.1. Radiation balance

Knowing that the reaction rate in a photoinduced process is proportional to the number of suitable absorbed photons by the catalyst, it is clear that the description of the number of photons absorbed by the system is crucial. Many rigorous and simplistic models have been proposed to describe the absorption of photons through the reactor. This absorbed useful energy has been defined in the literature through a property called the Local Volumetric Rate of Energy Absorption (LVREA) [76].

Depending on the physical properties of the reactor, the LVREA can be calculated via solving the radiation transport equation (RTE), the Zero Scattering or Zero Reflectance Model (ZRM) [77], the Two Flux Model (TFM) [78], or the Six Flux Model (SFM) [79]. The rigorous solution of the RTE is usually achieved by probabilistic methods such as Monte Carlo simulations [80], or discretization methods [81]. However, the solution of such a model is complex and highly computational demanding [79]; thus, more simple models such as the ZSM, TFM, and SFM are usually employed.

The ZRM [77], also called the Lambert-Beer model, is the simplest model of all and considers that the light passes through a fully homogeneous media and there is no photon reflection or scattering by particles. Although for homogeneous media the ZSM gives a good approximation, it overestimates the rate of photon absorption for non-homogeneous systems where the scattering effect cannot be neglected [82].

The TFM developed by Aketa et al [78] is a 1D model that assumes that when a photon hits a particle, scattering occurs only in the backward direction. Although this model presents a good approximation of the rate of photon absorption, according to Dal et al [60], the TFM is only suitable for low concentrations of solid particles where the scattering effect is not very significant. The TFM has been successfully applied and experimentally validated in flat-plate packed bed photoreactors [60], in slurry flat plate reactors [83] and slurry annular photoreactors [79,84].

Finally, the SFM proposed by Li Puma et al [79] and Brucato et al [83] is a 3D model that considers the effect of both light absorption and scattering. It estimates the absorption of photons considering probabilities to the photon scattering in the six principal directions. However, this model is much more complex as it considers the essence of the rigorous approach [84]. Figure 7 presents a schematic representation of the photon fluxes in the TFM and the six principal scattering directions in the SFM.

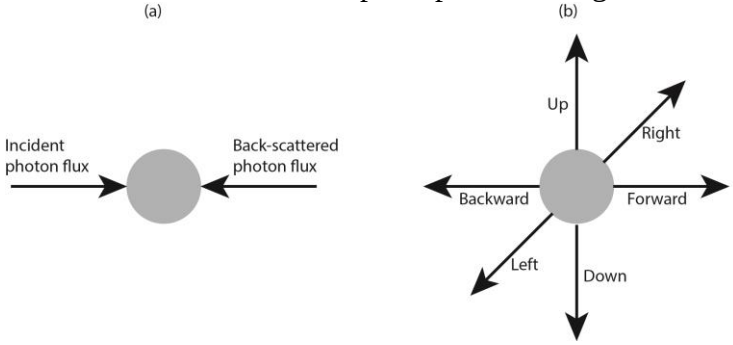

Figure 7: Schematic representation of (a) photon fluxes in the Two-Flux Model; (b) the six principal directions of photon scattering in the Six-Flux Model. (after [85]**)**

In a flat plate reactor with the catalyst film at the bottom of the reactor, the ZRM should describe accurately the radiation field [86]. In addition, to model the radiation field the following assumptions are made:

i. The incident radiant flux is vertical to the reactor
ii. The reactor is a perfect plane made of non-reflecting and non-absorbing materials
iii. The effect of the interface between photocatalyst and support is negligible
iv. The catalyst is coated uniformly on the support
v. The photocatalyst support is made of Pyrex-glass and is completely UVA transparent
vi. The light absorption and scattering of the continuous phase are negligible compared with the photocatalyst

The last assumption holds true due to the small thickness of the flat plate reactor and that the absorption coefficient of both water and phenol at the UVA wavelength are negligible [72]. Therefore, the exponential decay along the photocatalytic film, ignoring all possible scattering is described by the Lambert-Beer law:

$$E = E_o \exp(-\mu\sigma) \tag{3.1}$$

Where E_o is the initial photon flux, μ is the extinction coefficient, and σ is the film thickness that goes from 0 where the light enters the catalyst, to l_{gs} at the end of the catalytic film.

The local rate of photon absorption is then given by the gradient of light intensity in the direction of propagation:

$$e_a = -\frac{dE}{d\sigma} = \mu E_o \exp(-\mu\sigma) \tag{3.2}$$

And in dimensionless form:

$$E_a = \frac{e_a}{E_o \mu} \tag{3.3}$$

3.2. Photocatalyst modelling

To model the pollutant concentration along the photocatalytic film, the catalyst was described as a 1-D slab as illustrated in Figure 8.

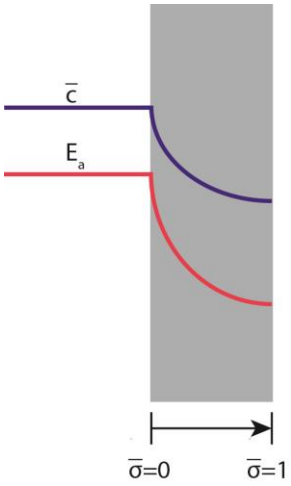

Figure 8: Schematic of the dimensionless concentration profile and the dimensionless rate of photon absorption along a 1D slab

Considering reaction and diffusion and steady state operation, the mathematical model to compute the pollutant concentration along the slab thickness is:

$$D_e \frac{d^2 C_A}{d\sigma^2} - r_A = 0 \tag{3.4}$$

With the boundary conditions:

$$C_A\big|_{\sigma=o} = C_{A,s} \tag{3.5}$$

$$\left.\frac{dC_A}{d\sigma}\right|_{\sigma=l_{gs}} = 0 \tag{3.6}$$

Where C_A is the concentration of the pollutant, r_A is the reaction rate, and the effective diffusivity, D_e, is given by:

$$D_e = D_\infty \frac{\varepsilon}{\tau} \tag{3.7}$$

Where ε is the porosity of the catalyst, τ is the tortuosity, and D_∞ is the diffusion coefficient.

The reaction rate term is assumed to follow the Langmuir-Hinshelwood profile with a dependence on the photon absorption rate:

$$-r_A = e_a^{\,n} \frac{k_r K C_{A,z=0}}{1 + K C_{A,z=0}} \tag{3.8}$$

Where k_r is the apparent reaction constant, K is the equilibrium adsorption constant, $C_{A,z=0}$ is the concentration at the surface of the catalyst, and the exponent n depends on the efficiency of the electron-hole formation and recombination at the surface of the catalyst and takes a value between 0.5 and 1 when the reaction is kinetically controlled [87].

To make Equation (3.4) dimensionless, two dimensionless numbers have to be defined: the dimensionless adsorption constant, ϕ, and the Thiele modulus, Θ. As the reaction rate follows a LHHW profile, the Thiele modulus proposed by Petersen [88] and Bischoff et al [89] was used and the term accounting for the light absorption was added.

$$\phi = KC_{A,s} \tag{3.9}$$

$$\Theta = \frac{\phi}{1+\phi}\left(\frac{l_{gs}^2 e_a{}^n k_r K}{2D_e\left(\phi - \ln\left(1+\phi\right)\right)}\right)^{0.5} \tag{3.10}$$

Thus, in dimensionless form, Equation (3.4) becomes:

$$\frac{d^2\bar{c}}{d\bar{\sigma}^2} - \Theta^2 \frac{\bar{c}}{1+\phi\bar{c}} = 0 \tag{3.11}$$

And the dimensionless boundary conditions:

$$\left.\frac{d\bar{c}}{d\bar{\sigma}}\right|_{\bar{\sigma}=1} = 0 \tag{3.12}$$

$$\bar{c}\big|_{\bar{\sigma}=0} = 1 \tag{3.13}$$

3.3. Fluid dynamic model and material balance along the reactor

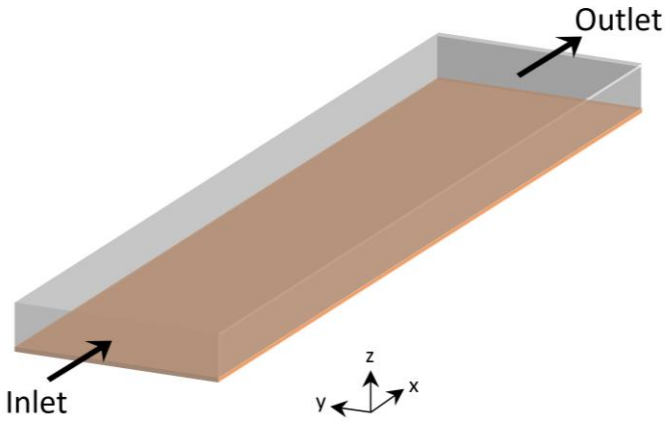

Figure 9: 3D view of the flat plate photoreactor with the film photocatalyst deposited at the bottom

The material balance for the pollutant in the reactor illustrated in Figure 9 is given by:

$$\frac{\partial C_A}{\partial t} = -\left(\nabla \cdot C_A \mathbf{v}\right) + \left(\nabla \cdot J_A\right) + R_A \tag{3.14}$$

Where C_A is the molar concentration of the pollutant, **v** is the fluid velocity vector, J_A is the diffusion molar flux, and R_A is the volumetric rate of reaction of A. Substituting Fick's law for a constant diffusivity, D, Equation (3.14) becomes:

$$\frac{\partial C_A}{\partial t} = -\left(\nabla \cdot C_A \mathbf{v}\right) + D\left(\nabla^2 C_A\right) + R_A \tag{3.15}$$

Which in rectangular coordinates is:

$$\frac{\partial C_A}{\partial t} = -\left[\frac{\partial\left(v_x C_A\right)}{\partial x} + \frac{\partial\left(v_y C_A\right)}{\partial y} + \frac{\partial\left(v_z C_A\right)}{\partial z}\right] + D\left(\frac{\partial^2 C_A}{\partial x^2} + \frac{\partial^2 C_A}{\partial y^2} + \frac{\partial^2 C_A}{\partial z^2}\right) + R_A \quad (3.16)$$

To model the material balance in the flat-plate photoreactor, the following assumptions are made:

i. Infinite plate in the *y* direction since the width of the reactor is many times the height of the reactor. As a result, the fluid velocity in the *y* direction is not present and no concentration gradients exist:

$$\frac{\partial\left(v_y C_A\right)}{\partial y} = 0 \quad (3.17)$$

$$D\frac{\partial^2 C_A}{\partial y^2} = 0 \quad (3.18)$$

ii. Fully developed laminar flow regime. Hence, the component v_z is equal to zero and v_x does not change in the axial direction:

$$\frac{\partial\left(v_z C_A\right)}{\partial z} = 0 \quad (3.19)$$

$$\frac{\partial\left(v_x C_A\right)}{\partial x} = v_x \frac{\partial C_A}{\partial x} \quad (3.20)$$

iii. Diffusion in the axial direction is negligible compared to the convection transport, therefore:

$$D\frac{\partial^2 C_A}{\partial x^2} = 0 \quad (3.21)$$

iv. Steady state operation:

$$\frac{\partial C_A}{\partial t} = 0 \quad (3.22)$$

v. The reaction occurs only on the surface of the catalyst; therefore, the reaction term is not present in Equation (3.16) and will be added as a boundary condition.

Under these assumptions, Equation (3.16) is simplified to:

$$-v_x \frac{\partial C_A}{\partial x} + D\frac{\partial^2 C_A}{\partial z^2} = 0 \quad (3.23)$$

The boundary conditions to solve Equation (3.23) are:

i. Pollutant adsorption and reaction on the catalytic surface:

$$D\left.\frac{\partial C_A}{\partial z}\right|_{z=0} = -r_A \quad (3.24)$$

ii. No flow through the top cover of the photoreactor:

$$\left.\frac{\partial C_A}{\partial z}\right|_{z=Z} = 0 \quad (3.25)$$

3.4. Numerical solution

The radiation profile, the pollutant profile along the photoreactor length, and the photocatalyst modelling were solved numerically in Matlab R2016a. The Matlab model to compute the radiation profile along the photocatalyst thickness is shown in Appendix A. The model of the steady state pollutant concentration along the photoreactor length is shown in Appendix B. Here, a 2D second order partial differential equation with boundary conditions has the be solved. This was achieved using the function *pdepe*. Finally, the model to analyse the photocatalyst film thickness is presented in Appendix C, where a second order ordinary differential equation with boundary conditions has to be solved. This was achieved by translating the second order differential equation into a system of two first order differential equations. Later, they were solved numerically using the function *bvp4c*.

4. Results and Discussion

4.1. Radiation field and photocatalyst modelling

Figure 10 presents the dimensionless photon absorption rate for different film thickness. The extinction coefficient to compute the photon absorption rate was assumed as that determined by Dal et al [60] for Degussa P25 titanium dioxide films and has a value of 10206 cm^{-1}. Figure 10 illustrates that increasing the film thickness augments the light absorption. For instance, for a thickness of 2µm, 13% of the incident light is still transmitted through the reactor wall, whereas when the film has a thickness of 5µm, just 1.7% of the incident light is transmitted through the reactor wall. Nonetheless, it is important to note that under these conditions, using a film thicker than 5µm has no positive results in the energy absorption as almost all light has already been absorbed.

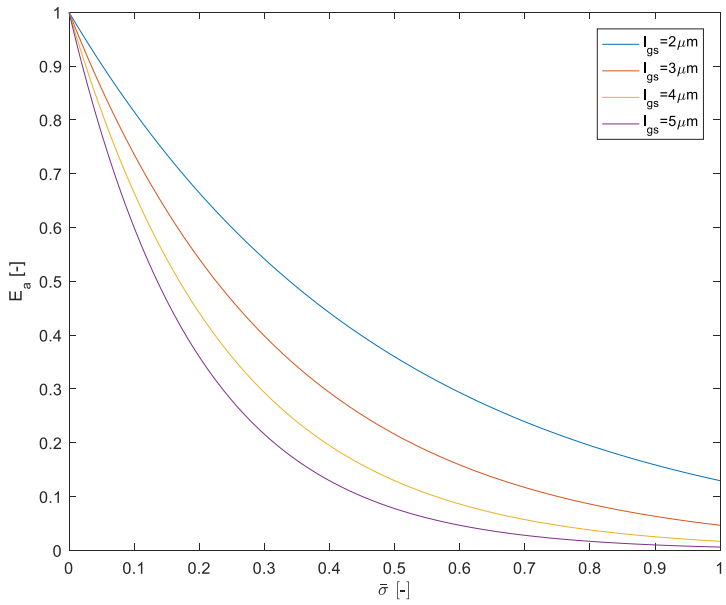

Figure 10: Dimensionless photon flux along the photocatalytic film thickness for different film thickness

In addition, increasing the film thickness may cause internal mass transfer limitations. To determine whether this is the case, the Thiele modulus was computed for each catalyst thickness assuming an initial concentration of pollutant of 1 mol m^{-3} and an initial irradiation of 25 W m^{-2}. The diffusion coefficient, reaction constant, and adsorption constant were assumed as those determined by Vezzoli et al [72] for the degradation of phenol: 9.1×10^{-10} m^2 s^{-1}, 0.5225×10^{-3} mol m^3 m^{-2} s^{-1} W^{-1}, and 0.85 m^3 mol^{-1}, respectively. To determine the effective diffusivity through the catalyst, a value of $\sqrt{3}$ was assigned to the tortuosity [90], while the porosity was assumed as 0.56 [72]. Thus, the effective diffusivity has a value of 2.929×10^{-10} m^2 s^{-1}. Finally, the reaction order with respect to the absorption of light, *n*, was assumed as 1 as the intensity used is well below the threshold value of 250 W m^2, where an order of 0.5 may be observed due to electron-hole recombination [21].

Substituting the aforestated values in Equation (3.10), the Thiele modulus are 0.1, 0.14, 0.18, and 0.22 for a film thickness of 2, 3, 4, and 5µm, respectively. As these values are well below 1, it can be assumed that there are no internal diffusion limitations [72]. Hereinafter, a value of 4µm will be adopted for the simulations due to its good light absorption and small internal diffusion limitations.

Figure 11 illustrates the dimensionless concentration for different film thickness (Figure 11a), different dimensionless equilibrium adsorption constant (Figure 11b), and different Thiele modulus (Figure 11c).

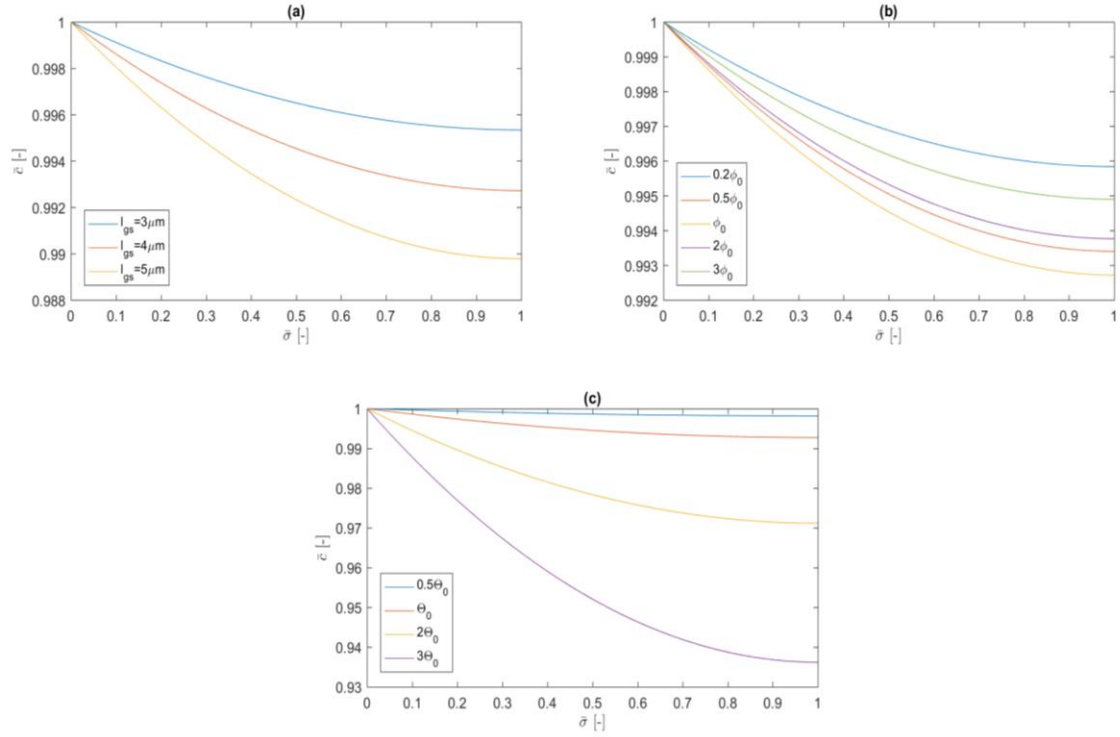

Figure 11: Dimensionless concentration profile along the catalyst film thickness for (a) different catalyst thickness; (b) different equilibrium adsorption constant for a catalyst thickness of 4µm; (c) different Thiele modulus for a catalyst thickness of 4µm.

From Figure 11a, it is noted that increasing the film thickness also increases the pollutant degradation along the catalyst as there is more surface area to react. Figure 11b illustrates that the equilibrium adsorption constant plays a major role in the pollutant degradation. For example, when its value is two times the base-case value, the concentration at the end of the slab is higher. Likewise, when its value is half of the base-case, the concentration at the end of the slab is also higher. In the former case, the adsorption constant is much higher compared to the desorption constant; hence, the desorption limits the overall reaction. In the latter case, the desorption constant is much higher compared to the adsorption constant; hence, the adsorption of the contaminant onto the catalyst limits the overall reaction. Therefore, the importance of effectively design and develop catalysts which facilitate both adsorption of the reactants and desorption of the products.

From Figure 11c, it is noted that when the Thiele modulus decreases by half compared to the base-scenario, the concentration profile along the slab is rather constant. On the other hand, when the Thiele modulus increases compared to the base-case scenario, the pollutant concentration decreases much faster. Analyzing

Equation (3.10), an increase in the Thiele modulus may be achieved by increasing the thickness of the catalytic film, increasing the irradiation intensity, or decreasing the effective diffusivity. However, it is important to maintain its value well below 1 as mentioned before to not have a diffusion limited reaction.

4.2. Photoreactor dimensions

To compute the length of the photoreactor, a volumetric flow rate of water to be treated of 0.5 m^3 day^{-1} was assumed with an initial concentration of phenol of 1 mol m^{-3}. It was also considered an average sunshine duration of 10 hours, an average incident UVA radiation of 25 W m^{-2}, an initial photoreactor height of 1 cm, and a photoreactor width of 40 cm.

Figure 12a illustrates a surface of the steady state concentration of the pollutant along the photoreactor, whereas Figure 12b illustrates the concentration profile along the photoreactor length at different layers of the photoreactor height, *z*. From both figures, it is noted that there is a radial concentration profile, where the concentration of the pollutant from the layers close to the catalyst diminishes fast, while the upper layers diffuse rather slow to where the reaction takes place. In addition, it is seen that for a single-pass reactor, to achieve approximately 95% conversion, the photoreactor length has to be around 60 meters.

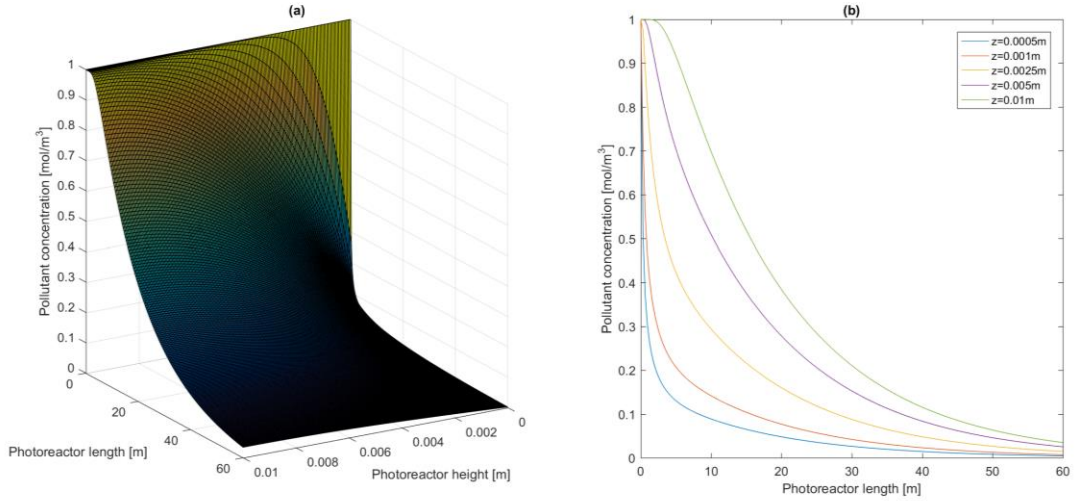

Figure 12: (a) Outline of the pollutant concentration along the photoreactor; (b) Pollutant concentration profile along the photoreactor length at different photoreactor heights, z.

Figure 13 presents the profile of the pollutant conversion at the top layer of the photoreactor along the photoreactor length for different values of reaction rates (Figure 13a) and different values of diffusion coefficient (Figure 13b). From Figure 12a, it is important to note that increasing the reaction rate by a factor of two or decreasing the reaction rate by half had little effect on the overall conversion along the photoreactor length. On the other hand, from Figure 13b, it is noted that the diffusion coefficient has a large effect on the overall conversion. For instance, when the diffusion coefficient was decreased by half of its initial value, 60 meters were not enough to reach 95% conversion of the pollutant, whereas when increasing the diffusion coefficient two times, the pollutant is fully degraded at around 40 meters. Therefore, in the modelled system, the diffusion of the pollutant from the bulk fluid onto the catalyst is what limits the overall reaction rate.

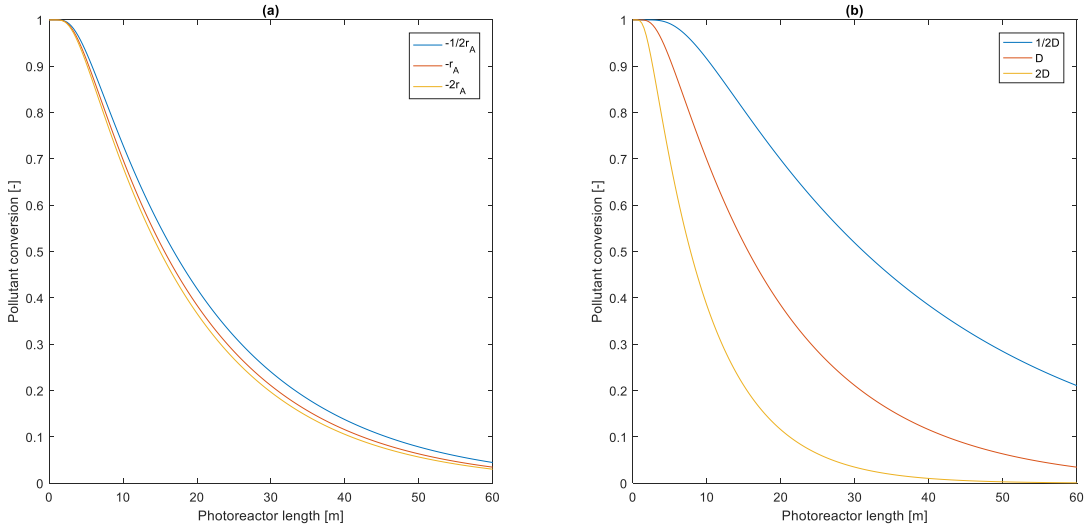

Figure 13: Outline of the pollutant conversion at the top area of the reactor along the reactor length for (a) different values of reaction rates, and (b) different values of the diffusion coefficient

So far, the photoreactor height has been fixed to 1 cm; however, as the external mass transfer from the bulk fluid onto the active catalyst film limits the overall reaction rate, to effectively design the photoreactor it is important to explore other reactor heights. Figure 14a presents the pollutant conversion at the top layer of the photoreactor at various reactor heights, whereas Figure 14b illustrates the residence time at some of those reactor heights to achieve 95% conversion. From Figure 14a, it is noted that decreasing the photoreactor height has a major effect in the pollutant conversion. For example, when the height was decreased from 1cm to 0.2cm, the photoreactor length was decreased from around 60 meters to less than 20 meters. Likewise, for a photoreactor height of 0.1cm the length to reach 95% conversion is around 10 meters. Moreover, from Figure 13b, it is noted that under the assumed properties, the optimal photoreactor height is below 0.45cm, as above that value the residence time in the reactor exceeds the 10 hours of sun light assumed.

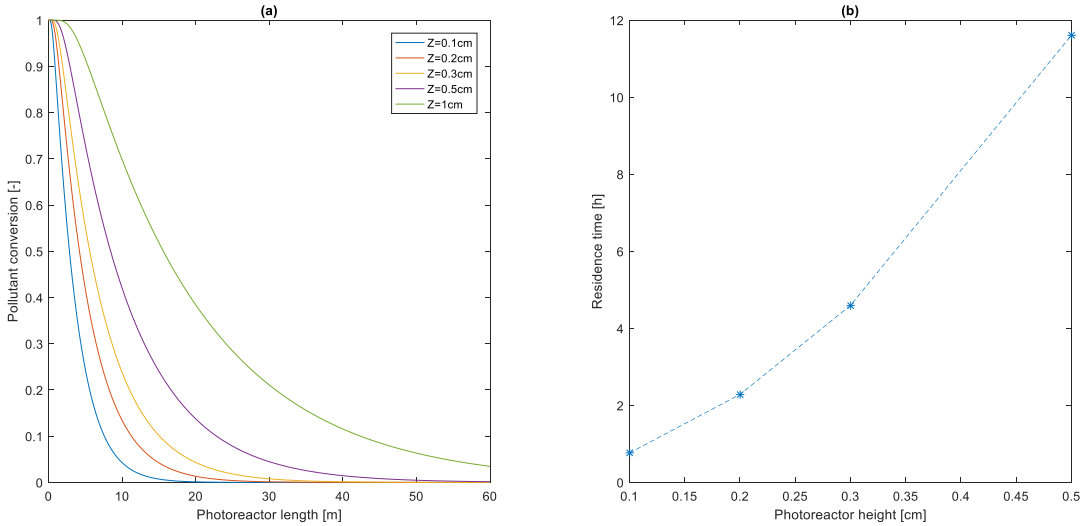

Figure 14: (a) Pollutant conversion varying the photoreactor height; (b) Residence time to achieve 95% conversion for different photoreactor height

In addition, Figure 15 presents the results of diminishing the photoreactor height even further. From Figure 15, it is noted that although decreasing the reactor height decreases the reactor length as the system is limited by external diffusion, there is a threshold value at which decreasing further the height has no further effect on the photoreactor length. For example, when the height of the photoreactor was decreased from 0.1cm to 0.01cm, the length to reach 95% conversion from around 10 meters to around 6 meters. In contrast, when the photoreactor height was decreased 0.01cm to 0.001cm, the length to reach 95% had no significant decrease; hence, at this point the system becomes kinetically controlled rather than diffusion controlled.

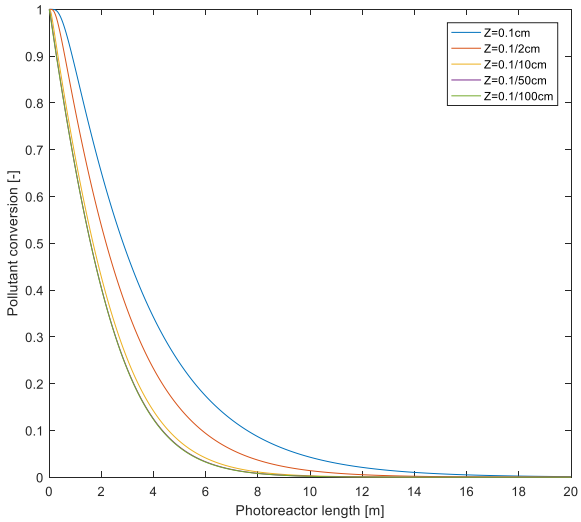

Figure 15: Limiting case of the pollutant conversion at different photoreactor heights

Finally, Figure 16 illustrates the effect of varying the photoreactor width on the photoreactor length at different heights to reach 95% conversion. Here, it is noted that decreasing the reactor width also diminishes the length of the reactor with a linear dependence. For example, at a photoreactor height of 0.1cm the reactor length for a width of 0.4m corresponds to approximately 10 meters. In contrast, at the same height and augmenting the width to 0.7m, the reactor length decreases approximately by half.

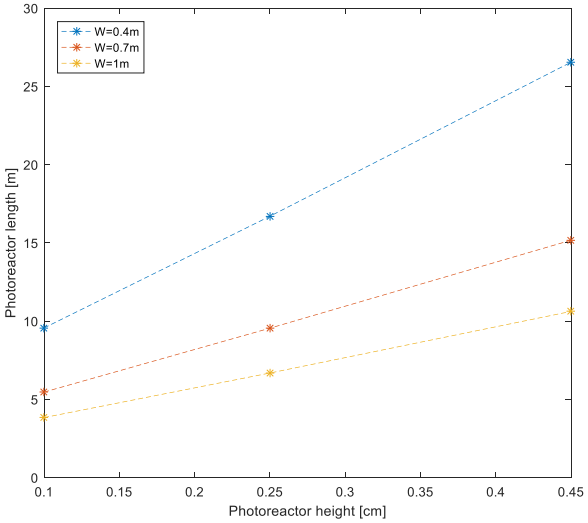

Figure 16: Photoreactor length to reach 95% conversion for different photoreactor height and width

5. Conclusions

A flat plate photoreactor with an immobilized film catalyst deposited at the bottom of the reactor to degrade phenol as target contaminant was modelled and designed. Based on a Zero Reflectance Model, and assuming there was no photon absorption or scattering by the bulk fluid, the local volumetric rate of energy absorption was computed along the photocatalyst film. The optimal film thickness was found at 4μm as above that value no positive effect on the absorption of energy was observed and no internal diffusion limitations were present.

It was noted that for a flat plate fixed film photoreactor, external diffusion of the pollutant from the bulk fluid onto the active catalyst is what limits the overall phenol degradation. Initially, for a reactor height of 1cm, the photoreactor length to reach 95% at the top layer of the reactor was around 60 meters. However, when the reactor height was diminished, the length of the reactor also decreased until a point where the system became kinetically controlled. As the assumed sunlight time was 10 hours, the photoreactor height to fulfil the required residence time had to be below 0.45cm, corresponding to a reactor length of around 25 meters. In contrast, a reactor height of 0.1cm had a corresponding reactor length of approximately 10 meters.

Acknowledgments

I wish to express my gratitude to Dominik Benz, who was my daily supervisor throughout this 2-month project. Dominik, without your valuable comments about my literature review, this report would be of much less quality. I also wish to express my gratitude to Dr. Ruud van Ommen from the Product and Process Engineering Department, who was my project supervisor. Ruud, thank you for giving me the opportunity to do my System Integration Project in photocatalysis; a project which helped me discover my interest for the topic to the extent of wanting to pursue a master thesis project on it. Also, thank you for your thorough and fruitful comments on the outcomes of this project.

Notation

$\bar{c}$	Dimensionless pollutant concentration
C_A	Pollutant concentration (mol m^{-3})
D	Diffusion coefficient (m^2 s^{-1})
D_e	Effective diffusivity (m^2 s^{-1})
e_a	Rate of photon absorption (W m^{-3})
E_a	Dimensionless rate of photon absorption
h	Depth (m)
J	Diffusion flux (mol $m^{-2}s^{-1}$)
k_r	Apparent rate constant (mol m^3 m^{-2} s^{-1} W^{-1})
K	Adsorption equilibrium constant (m^3 mol^{-1})
l_{gs}	Thickness of the catalytic film layer (µm)
n	Order of the reaction with respect to the photon absorption
r_A	Reaction rate per unit surface area (mol s^{-1} m^{-2})
R_A	Volumetric reaction rate of the pollutant (mol s^{-1} m^{-3})
v	Liquid velocity (m s^{-1})
$\mathbf{v}$	Velocity vector (m s^{-1})
x	Axial direction, photoreactor length (m)
y	Lateral direction, photoreactor width (m)
z	Vertical direction, photoreactor height (m)
Z	Flat plate photoreactor height (m)

Greek letters

ε	Catalyst porosity
Θ	Thiele modulus
μ	Extinction coefficient (m^{-1})
σ	Photocatalyst film thickness (m)
$\bar{\sigma}$	Dimensionless photocatalyst film thickness
τ	Catalyst tortuosity
ϕ	Dimensionless equilibrium adsorption constant

Special characters

∇	Vector differential operator
$\langle\ \rangle$	Mean value
∂	Differential operator

Bibliography

[1] The Human Right to Water and Sanitation, (1989).

[2] D. Mazhindu, Shared responsibility., 2014. doi:10.7748/nm.21.4.12.s12.

[3] M.N. Chong, B. Jin, C.W.K. Chow, C. Saint, Recent developments in photocatalytic water treatment technology: A review, Water Res. 44 (2010) 2997–3027. doi:10.1016/j.watres.2010.02.039.

[4] S. Malato, P. Ferná Ndez-Ibá Ñ Ez, M.I. Maldonado, J. Blanco, W. Gernjak, Decontamination and disinfection of water by solar photocatalysis: Recent overview and trends, (n.d.). doi:10.1016/j.cattod.2009.06.018.

[5] A. Gadgil, DRINKING WATER IN DEVELOPING COUNTRIES, Annu. Rev. Energy Env. 23 (1998) 253–86.

[6] L. Prieto-Rodriguez, S. Miralles-Cuevas, I. Oller, A. Agüera, G.L. Puma, S. Malato, Treatment of emerging contaminants in wastewater treatment plants (WWTP) effluents by solar photocatalysis using low TiO2 concentrations, J. Hazard. Mater. 211-212 (2012) 131–137. doi:10.1016/j.jhazmat.2011.09.008.

[7] N. Bolong, A.F. Ismail, M.R. Salim, T. Matsuura, A review of the effects of emerging contaminants in wastewater and options for their removal, Desalination. 239 (2009) 229–246. doi:10.1016/j.desal.2008.03.020.

[8] J.E. Duran, M. Mohseni, F. Taghipour, Computational fluid dynamics modeling of immobilized photocatalytic reactors for water treatment, AIChE J. 57 (2011) 1860–1872. doi:10.1002/aic.12399.

[9] P.-D. Hansen, Risk assessment of emerging contaminants in aquatic systems, TrAC Trends Anal. Chem. 26 (2007) 1095–1099. doi:10.1016/j.trac.2007.10.001.

[10] P.V.A. Padmanabhan, K.P. Sreekumar, T.K. Thiyagarajan, R.U. Satpute, K. Bhanumurthy, P. Sengupta, G.K. Dey, K.G.K. Warrier, Nano-crystalline titanium dioxide formed by reactive plasma synthesis, Vacuum. 80 (2006) 1252–1255. doi:10.1016/j.vacuum.2006.01.054.

[11] K.-H. Wang, Y.-H. Hsieh, M.-Y. Chou, C.-Y. Chang, Photocatalytic degradation of 2-chloro and 2-nitrophenol by titanium dioxide suspensions in aqueous solution, Appl. Catal. B Environ. 21 (1999) 1–8. doi:10.1016/S0926-3373(98)00116-7.

[12] P.R. Gogate, A.B. Pandit, A review of imperative technologies for wastewater treatment I: oxidation technologies at ambient conditions, Adv. Environ. Res. 8 (2004) 501–551. doi:10.1016/S1093-0191(03)00032-7.

[13] U.I. Gaya, A.H. Abdullah, Heterogeneous photocatalytic degradation of organic contaminants over titanium dioxide: A review of fundamentals, progress and problems, J. Photochem. Photobiol. C Photochem. Rev. 9 (2008) 1–12. doi:10.1016/j.jphotochemrev.2007.12.003.

[14] M.A. Fox, Organic heterogeneous photocatalysis: chemical conversions sensitized by irradiated semiconductors, Acc. Chem. Res. 16 (1983) 314–321. doi:10.1021/ar00093a001.

[15] R. Jolley, L. Condie, J. Johnson, S. Katz, Water chlorination: chemistry, environmental impact and health effects, Impact Heal. …. (1990). http://bases.bireme.br/cgi-bin/wxislind.exe/iah/online/?IsisScript=iah/iah.xis&src=google&base=REPIDISCA&lang=p&nextAction=lnk&exprSearch=78795&indexSearch=ID (accessed May 29, 2016).

[16] O. Carp, C.L. Huisman, A. Reller, Photoinduced reactivity of titanium dioxide, Prog. Solid State Chem. 32 (2004) 33–177. doi:10.1016/j.progsolidstchem.2004.08.001.

[17] L. Prieto-Rodriguez, S. Miralles-Cuevas, I. Oller, A. Ag??era, G.L. Puma, S. Malato, Treatment of emerging contaminants in wastewater treatment plants (WWTP) effluents by solar photocatalysis using low TiO 2 concentrations, J. Hazard. Mater. 211-212 (2012) 131–137. doi:10.1016/j.jhazmat.2011.09.008.

[18] D. Chen, M. Sivakumar, A.K. Ray, Heterogeneous Photocatalysis in Environmental Remedia tion, Dev. Chem. Eng. Miner. Process. 8 (2000) 505–550. doi:10.1002/apj.5500080507.

[19] D.M. Blake, P.-C. Maness, Z. Huang, E.J. Wolfrum, J. Huang, W.A. Jacoby, Application of the Photocatalytic Chemistry of Titanium Dioxide to Disinfection and the Killing of Cancer Cells, Sep. Purif. Rev. 28 (1999) 1–50. doi:10.1080/03602549909351643.

[20] N. Zhang, Y. Zhang, Y.-J. Xu, Recent progress on graphene-based photocatalysts: current status and future perspectives, Nanoscale. 4 (2012) 5792. doi:10.1039/c2nr31480k.
[21] J.-M. Herrmann, Heterogeneous photocatalysis: state of the art and present applications In honor of Pr. R.L. Burwell Jr. (1912–2003), Former Head of Ipatieff Laboratories, Northwestern University, Evanston (Ill)., Top. Catal. 34 (2005) 49–65. doi:10.1007/s11244-005-3788-2.
[22] Z. Li, LED-Based Photocatalytic Reactor Design, Delft University of Technology, 2016.
[23] M. Motegh, Design of Photocatalytic Reactors, Delft University of Technology, 2013.
[24] T. Van Gerven, G. Mul, J. Moulijn, A review of intensification of photocatalytic processes, Chem. Eng. Process. Process Intensif. 46 (2007) 781–789. doi:10.1016/j.cep.2007.05.012.
[25] N. Huang, X. Min-hua, C. Yuan, Y. Rui-rong, The study of the photokilling effect and mechanism of ultrafine TiO2 particles on U937 cells, J. Photochem. Photobiol. A Chem. 108 (1997) 229–233. doi:10.1016/S1010-6030(97)00093-2.
[26] R. Cai, Y. Kubota, T. Shuin, H. Sakai, K. Hashimoto, A. Fujishima, Induction of cytotoxicity by photoexcited TiO2 particles., Cancer Res. 52 (1992) 2346–8. http://www.ncbi.nlm.nih.gov/pubmed/1559237 (accessed May 29, 2016).
[27] A. Mills, S. Le Hunte, An overview of semiconductor photocatalysis, J. Photochem. Photobiol. A Chem. 108 (1997) 1–35. doi:10.1016/S1010-6030(97)00118-4.
[28] C. Chan, K. Wong, W. Chung, Photocatalytic degradation of di (2-ethylhexyl) phthalate adsorbed by chitin A, Water Sci. (2007). https://www.researchgate.net/profile/Po_Keung_Wong/publication/5893622_Photocatalytic_Degradation_of_di(2-ethylhexyl)Phthalate_Adsorbed_by_Chitin_A/links/54d2bc200cf2b0c6146bca45.pdf (accessed May 29, 2016).
[29] C.B. Almquist, P. Biswas, Role of Synthesis Method and Particle Size of Nanostructured TiO2 on Its Photoactivity, J. Catal. 212 (2002) 145–156. doi:10.1006/jcat.2002.3783.
[30] D. Bennett, University of California at Davis: Catalysis, (2015). http://chemwiki.ucdavis.edu/Textbook_Maps/General_Chemistry_Textbook_Maps/Map%3A_Chemistry_(OpenSTAX)/12%3A_Kinetics/12.8%3A_Catalysis (accessed May 28, 2016).
[31] O. Ola, M. Maroto-Valer, D. Liu, S. MacKintosh, C.W. Lee, J.C.S. Wu, Performance comparison of CO 2 conversion in slurry and monolith photoreactors using Pd and Rh-TiO 2 catalyst under ultraviolet irradiation, Appl. Catal. B Environ. 126 (2012) 172–179. doi:10.1016/j.apcatb.2012.07.024.
[32] M.F.. Dijkstra, A. Michorius, H. Buwalda, H.. Panneman, J.G.. Winkelman, A.A.C.. Beenackers, Comparison of the efficiency of immobilized and suspended systems in photocatalytic degradation, Catal. Today. 66 (2001) 487–494. doi:10.1016/S0920-5861(01)00257-7.
[33] S. Gelover, L.A. Gó Mez, K. Reyes, M.T. Leal, S. Tio, A practical demonstration of water disinfection using TiO 2 films and sunlight Coliforms Bacterial regrowth, (2006). doi:10.1016/j.watres.2006.07.006.
[34] T.-T. Lim, P.-S. Yap, M. Srinivasan, A.G. Fane, TiO_2 /AC Composites for Synergistic Adsorption-Photocatalysis Processes: Present Challenges and Further Developments for Water Treatment and Reclamation, Crit. Rev. Environ. Sci. Technol. 41 (2011) 1173–1230. doi:10.1080/10643380903488664.
[35] R.K. Upadhyay, N. Soin, S.S. Roy, Role of graphene/metal oxide composites as photocatalysts, adsorbents and disinfectants in water treatment: a review, RSC Adv. 4 (2014) 3823. doi:10.1039/c3ra45013a.
[36] R.W. Matthews, Hydroxylation Reactions Induced by Near-ultraviolet Photolysis of Aqueous Titanium Dioxide Suspensions, J. Chem. SOC. Faraday Trans. I. 80 (1984).
[37] C.D. Jaeger, A.J. Bard, Spin trapping and electron spin resonance detection of radical intermediates in the photodecomposition of water at titanium dioxide particulate systems, J. Phys. Chem. 83 (1979) 3146–3152. doi:10.1021/j100487a017.
[38] C.S. Turchi, D.F. Ollis, Photocatalytic Degradation of Organic Water Contaminants: Mechanisms Involving Hydroxyl Radical Attack, J. Catal. 122 (1990) 178–192.
[39] G. Yang, Z. Jiang, H. Shi, T. Xiao, Z. Yan, Preparation of highly visible-light active N-doped TiO2 photocatalyst, J. Mater. Chem. 20 (2010) 5301. doi:10.1039/c0jm00376j.

[40] I.N. Martyanov, S. Uma, S. Rodrigues, K.J. Klabunde, Structural defects cause TiO2-based photocatalysts to be active in visible light, Chem. Commun. 95 (2004) 2476. doi:10.1039/b409730k.
[41] T. Jiang, L. Zhang, M. Ji, Q. Wang, Q. Zhao, X. Fu, H. Yin, Carbon nanotubes/TiO2 nanotubes composite photocatalysts for efficient degradation of methyl orange dye, Particuology. 11 (2013) 737–742. doi:10.1016/j.partic.2012.07.008.
[42] B. Neppolian, A. Bruno, C.L. Bianchi, M. Ashokkumar, Graphene oxide based Pt–TiO2 photocatalyst: Ultrasound assisted synthesis, characterization and catalytic efficiency, Ultrason. Sonochem. 19 (2012) 9–15. doi:10.1016/j.ultsonch.2011.05.018.
[43] A. Rahman Mohamed, T.S. H, M.A. R, Synthesis and characterization of CNT/Ce-TiO 2 nanocomposite for phenol degradation, J. Rare Earths. 30 (2012) 651–658. doi:10.1016/S1002-0721(12)60107-0.
[44] Y. Gou, D. Chen, Z. Su, Photocatalyst of nanometer TiO2/conjugated polymer complex employed for depigmentation of methyl orange, Appl. Catal. A Gen. 261 (2004) 15–18. doi:10.1016/j.apcata.2003.10.048.
[45] M.D. Stoller, S. Park, Y. Zhu, J. An, R.S. Ruoff, Graphene-Based Ultracapacitors, Nano Lett. 8 (2008) 3498–3502. doi:10.1021/nl802558y.
[46] X. Li, Y. Zhu, W. Cai, M. Borysiak, B. Han, D. Chen, R.D. Piner, L. Colombo, R.S. Ruoff, Transfer of Large-Area Graphene Films for High-Performance Transparent Conductive Electrodes, Nano Lett. 9 (2009) 4359–4363. doi:10.1021/nl902623y.
[47] J.-U. Lee, D. Yoon, H. Cheong, Estimation of Young's Modulus of Graphene by Raman Spectroscopy, Nano Lett. 12 (2012) 4444–4448. doi:10.1021/nl301073q.
[48] A.A. Balandin, Thermal properties of graphene and nanostructured carbon materials, Nat. Mater. 10 (2011) 569–581. doi:10.1038/nmat3064.
[49] A.S. Mayorov, R. V. Gorbachev, S. V. Morozov, L. Britnell, R. Jalil, L.A. Ponomarenko, P. Blake, K.S. Novoselov, K. Watanabe, T. Taniguchi, A.K. Geim, Micrometer-Scale Ballistic Transport in Encapsulated Graphene at Room Temperature, Nano Lett. 11 (2011) 2396–2399. doi:10.1021/nl200758b.
[50] I. Salvadó-Estivill, A. Brucato, G.L. Puma, Two-Dimensional Modeling of a Flat-Plate Photocatalytic Reactor for Oxidation of Indoor Air Pollutants, (n.d.). doi:10.1021/ie070391r.
[51] T.H. Lim, S.D. Kim, Trichloroethylene degradation by photocatalysis in annular flow and annulus fluidized bed photoreactors, Chemosphere. 54 (2004) 305–312. doi:10.1016/S0045-6535(03)00753-7.
[52] M.M. Hossain, G.B. Raupp, S.O. Hay, T.N. Obee, Three-dimensional developing flow model for photocatalytic monolith reactors, AIChE J. 45 (1999) 1309–1321. doi:10.1002/aic.690450615.
[53] H.. Yatmaz, C. Wallis, C.. Howarth, The spinning disc reactor – studies on a novel TiO2 photocatalytic reactor, Chemosphere. 42 (2001) 397–403. doi:10.1016/S0045-6535(00)00088-6.
[54] C. McCullagh, N. Skillen, M. Adams, P.K.J. Robertson, Photocatalytic reactors for environmental remediation: A review, J. Chem. Technol. Biotechnol. 86 (2011) 1002–1017. doi:10.1002/jctb.2650.
[55] M. Tahir, N.S. Amin, Recycling of carbon dioxide to renewable fuels by photocatalysis: Prospects and challenges, Renew. Sustain. Energy Rev. 25 (2013) 560–579. doi:10.1016/j.rser.2013.05.027.
[56] A. Alexiadis, I. Mazzarino, Design guidelines for fixed-bed photocatalytic reactors, Chem. Eng. Process. Process Intensif. 44 (2005) 453–459. doi:10.1016/j.cep.2004.06.009.
[57] D.W. Chen, F.M. Li, A.K. Ray, Effect of mass transfer and catalyst layer thickness on photocatalytic reaction, Aiche J. 46 (2000) 1034–1045. doi:10.1002/aic.690460515.
[58] H. Lu, M.A. Schmidt, K.F. Jensen, Photochemical Reactions and Online Product Detection in Microfabricated Reactors, in: Microreact. Technol., Springer Berlin Heidelberg, Berlin, Heidelberg, 2001: pp. 175–184. doi:10.1007/978-3-642-56763-6_19.
[59] G.H. Rossetti, E.D. Albizzati, O.M. Alfano, Modeling and Experimental Verification of a Flat-Plate Solar Photoreactor, (n.d.).
[60] Z. Dal, M. Gu, A. Chen, H. Gu, Z. Zhu, Modeling and experimental verification of radiative transfer of a flat-plate photoreactor with immobilized photocatalyst, J. Chem. Technol. Biotechnol. 77 (2002) 1127–1133. doi:10.1002/jctb.686.

[61] Y. İnel, A.N. Ökte, Photocatalytic degradation of malonic acid in aqueous suspensions of titanium dioxide: an initial kinetic investigation of CO2 photogeneration, J. Photochem. Photobiol. A Chem. 96 (1996) 175–180. doi:10.1016/1010-6030(95)04288-1.
[62] R.W. Matthews, Photocatalytic oxidation of organic contaminants in water: An aid to environmental preservation, Pure Appl. Chem. 64 (1992) 1285–1290. doi:10.1351/pac199264091285.
[63] S.T. Martin, A.T. Lee, M.R. Hoffmann, Chemical mechanism of inorganic oxidants in the TiO2/UV process: increased rates of degradation of chlorinated hydrocarbons, Environ. Sci. Technol. 29 (1995) 2567–2573. doi:10.1021/es00010a017.
[64] A.-G. Rincón, C. Pulgarin, Effect of pH, inorganic ions, organic matter and H 2 O 2 on E. coli K12 photocatalytic inactivation by TiO 2 Implications in solar water disinfection, Appl. Catal. B Environ. 51 (2004) 283–302. doi:10.1016/j.apcatb.2004.03.007.
[65] Y. Wang, C.-S. Hong, TiO2-mediated photomineralization of 2-chlorobiphenyl: the role of O2, Water Res. 34 (2000) 2791–2797. doi:10.1016/S0043-1354(00)00009-9.
[66] A. Sobczyński, A. Dobosz, Water Purification by Photocatalysis on Semiconductors, Polish J. Environ. Stud. 10 (2001) 195–205.
[67] L. Cermenati, A. Albini, P. Pichat, C. Guillard, TiO2 photocatalytic degradation of haloquinolines in water: Aromatic products GM-MS identification. Role of electron transfer and superoxide, Res. Chem. Intermed. 26 (2000) 221–234. doi:10.1163/156856700X00741.
[68] A. Sobczyński, L. Duczmal, W. Zmudziński, Phenol destruction by photocatalysis on TiO2: An attempt to solve the reaction mechanism, J. Mol. Catal. A Chem. 213 (2004) 225–230. doi:10.1016/j.molcata.2003.12.006.
[69] J. Klanova, P. Klan, J. Nosek, I. Holoubek, Environmental ice photochemistry: Monochlorophenols, Environ. Sci. Technol. 37 (2003) 1568–1574. doi:10.1021/es025875n.
[70] S.T. Martin, H. Herrmann, W. Choi, M.R. Hoffmann, Time-resolved microwave conductivity. Part 1.—TiO 2 photoreactivity and size quantization, J. Chem. Soc., Faraday Trans. 90 (1994) 3315–3322. doi:10.1039/FT9949003315.
[71] K. Vinodgopal, U. Stafford, K.A. Gray, P. V. Kamat, Electrochemically Assisted Photocatalysis. 2. The Role of Oxygen and Reaction Intermediates in the Degradation of 4-Chlorophenol on Immobilized TiO2 Particulate Films, (2002).
[72] M. Vezzoli, T. Farrell, A. Baker, S. Psaltis, W.N. Martens, J.M. Bell, Optimal catalyst thickness in titanium dioxide xed lm reactors: mathematical modelling and experimental validation, (n.d.).
[73] A.E. Cassano, C.A. Martin, R.J. Brandi, O.M. Alfano, Photoreactor Analysis and Design: Fundamentals and Applications, Ind. Eng. Chem. Res. 34 (1995) 2155–2201. doi:10.1021/ie00046a001.
[74] M. Vezzoli, Intrinsic kinetics of titania photocatalysis : Simplified Models for their investigation by, (2012). http://eprints.qut.edu.au/51574/1/Massimiliano_Vezzoli_Thesis.pdf.
[75] L. Yang, Z. Liu, J. Shi, H. Hu, W. Shangguan, Design consideration of photocatalytic oxidation reactors using TiO2-coated foam nickels for degrading indoor gaseous formaldehyde, Catal. Today. 126 (2007) 359–368. doi:10.1016/j.cattod.2007.06.017.
[76] A.E. Cassano, C.A. Martin, B.R. J., O.M. Alfano, Photoreactor Analysis and Design : Fundamentals and Applications, Ind. Eng. Chem. Res. 34 (1995) 2155–2201. doi:10.1021/ie00046a001.
[77] A. Brucato, L. Rizzuti, Simplified Modeling of Radiant Fields in Heterogeneous Photoreactors . 1 . Case of Zero Reflectance, Ind. Eng. Chem. Res. 36 (1997) 4740–4747. http://pubs.acs.org/doi/abs/10.1021/ie960259j.
[78] A. T., Light intensity profiles in bubble-dispersed systems: An approach to the analysis of heterogeneous photoreactors, Kagaku Kogaku Ronbunshu. 2 (1976) 583–588.
[79] G. Li Puma, J.N. Khor, A. Brucato, Modeling of an annular photocatalytic reactor for water purification: Oxidation of pesticides, Environ. Sci. Technol. 38 (2004) 3737–3745. doi:10.1021/es0301020.
[80] M. Pasquali, F. Santarelli, J.F. Porter, P.-L. Yue, Radiative Transfer in Photocatalytic Systems, (n.d.).
[81] J. Moreira, B. Serrano, A. Ortiz, H. de Lasa, Evaluation of Photon Absorption in an Aqueous TiO_2 Slurry Reactor Using Monte Carlo Simulations and Macroscopic

Balance, Ind. Eng. Chem. Res. 49 (2010) 10524–10534. doi:10.1021/ie100374f.
[82] A. Brucato, A.E. Cassano, F. Grisafi, G. Montante, L. Rizzuti, G. Vella, Estimating radiant fields in flat heterogeneous photoreactors by the six-flux model, AIChE J. 52 (2006) 3882–3890. doi:10.1002/aic.10984.
[83] A. Brucato, A.E. Cassano, F. Grisafi, G. Montante, L. Rizzuti, G. Vella, Estimating radiant fields in flat heterogeneous photoreactors by the six-flux model, AIChE J. 52 (2006) 3882–3890. doi:10.1002/aic.10984.
[84] J. Colina-M??rquez, F. Machuca-Mart??nez, G. Li Puma, Photocatalytic mineralization of commercial herbicides in a pilot-scale solar CPC reactor: Photoreactor modeling and reaction kinetics constants independent of radiation field, Environ. Sci. Technol. 43 (2009) 8953–8960. doi:10.1021/es902004b.
[85] G. Li Puma, A. Brucato, Dimensionless analysis of slurry photocatalytic reactors using two-flux and six-flux radiation absorption–scattering models, Catal. Today. 122 (2007) 78–90. doi:10.1016/j.cattod.2007.01.027.
[86] M. Roger, J. Villermaux, Modelling of light absorption in photoreactors Part I. General formulation based on the laws of photometry, Chem. Eng. J. 17 (1979) 219–226. doi:10.1016/0300-9467(79)80106-9.
[87] W.A. Jacoby, D.M. Blake, R.D. Noble, C.A. Koval, Kinetics of the Oxidation of Trichloroethylene in Air via Heterogeneous Photocatalysis, J. Catal. 157 (1995) 87–96. doi:10.1006/jcat.1995.1270.
[88] E.E. Petersen, A general criterion for diffusion influenced chemical reactions in porous solids, Chem. Eng. Sci. 20 (1965) 587–591.
[89] K.B. Bischoff, Effectiveness factors for general reaction rate forms, AIChE J. 11 (1965) 351–355. doi:10.1002/aic.690110229.
[90] M.F.J. Dijkstra, H.J. Panneman, J.G.M. Winkelman, J.J. Kelly, A.A.C.M. Beenackers, Modeling the photocatalytic degradation of formic acid in a reactor with immobilized catalyst, Chem. Eng. Sci. 57 (2002) 4895–4907. doi:10.1016/S0009-2509(02)00290-7.

Appendix A: Radiation model

```
function ZRM_photoreactor
clc
clear
%Lambert Beer law
Eo=1;%irradiation, dimensionless
E=25;%W/m2 irradiation
alpha=1.0222;%um-1 Extinction coefficient film
a=1.0222e6;%m-1 ectinction coefficient for ea

%Different film thickness:
th1=2;%um
th2=3;%um
th3=4;%um
th4=5;%um

x1=0:0.01:th1;
x2=0:0.01:th2;
x3=0:0.01:th3;
x4=0:0.01:th4;

l1=x1./th1;
l2=x2./th2;
l3=x3./th3;
l4=x4./th4;
%Lambert beer law:
E1=Eo*exp(-alpha*x1);
E2=Eo*exp(-alpha*x2);
E3=Eo*exp(-alpha*x3);
E4=Eo*exp(-alpha*x4);

%Energy absorption
ea1=a*E*exp(-alpha*x1);
Ea1=ea1/(E*a);
ea2=a*E*exp(-alpha*x2);
Ea2=ea2/(E*a);
ea3=a*E*exp(-alpha*x3);
Ea3=ea3/(E*a);
ea4=a*E*exp(-alpha*x4);
Ea4=ea4/(E*a);
figure(1) %Photon absorption
plot(l1,Ea1)
hold on
plot(l2,Ea2)
hold on
plot(l3,Ea3)
hold on
plot(l4,Ea4)
hold on
legend('l_{gs}=2\mum','l_{gs}=3\mum','l_{gs}=4\mum','l_{gs}=5\mum')
xlabel('$\bar{\sigma}$ [-]','Interpreter','latex')
ylabel('E_{a} [-]')

end
```

Appendix B: Photoreactor length: steady state

```
%% Model of a photoreactor to compute the length at steady state
conditions
%The equation to be solved is: -v*dC/dx+D*d^2C/dz^2=0
%with the boundary conditions: at the top of the reactor dC/dz=0
%and at the bottom the reaction: D*dC/dz=-rA (the reaction takes
place)
function model_photoreactor_length
clear
clc

%% Reactor dimensions
global H; %height of the reactor
H=0.01; %m
global L; %length of the reactor
L=60;
global W;%width of the reactor
W=0.4;
Water=0.05;%flow in m3 per day
t_sun=10;%assuming 10 hours of sun per day
global Q;
Q=Water/(t_sun*3600); %m3/s of water to be treated
%% Physicochemical properties
global D;
D=9.1e-10; %diffusion coefficient [m2/s]
global Cao;
Cao=1; %mol/m3
global th;
th=4e-6;%catalytic film thickness [m]
global alpha;
alpha=1.02e6;%[m-1] Extinction coefficient film
global E;
E=25;% Intensity W/m2
global n;
n=1; %reaction order with respect to the light absorption
global k;
k=0.5226e-3; % reaction constant molm^2/m^2sW
global KA;
KA=0.85;% adsorption contant m3/mol

%% Solution
m=0; %for the flat plate (cartesian coordinates)
zmesh=linspace(0,H,200); %thickness of the photoreactor [m]
xspan=linspace(0,L,200); %length of the photoreactor [m]
sol=pdepe(m,@pdefun,@pdeic,@pdebc,zmesh,xspan);
u=sol(:,:,1);

    subplot(1,2,1)
        surf(zmesh,xspan,u)
        xlabel('Photoreactor height [m]')
        ylabel('Photoreactor length [m]')
        zlabel('Pollutant concentration [mol/m^3]')
        title('(a)')
    subplot(1,2,2)
        plot(xspan(end,:),u(:,10))
        hold on
        plot(xspan(end,:),u(:,20))
        hold on
        plot(xspan(end,:),u(:,50))
```

```
        hold on
        plot(xspan(end,:),u(:,100))
        hold on
        plot(xspan(end,:),u(:,end))
        %title('Conversion profile at different depths')
        xlabel('Photoreactor length [m]')
        ylabel('Pollutant concentration [mol/m^3]')
        legend('z=0.0005m', 'z=0.001m', 'z=0.0025m',
'z=0.005m','z=0.01m')
        title('(b)')
end
%% Function to be solved
function[c,f,s]=pdefun(x,t,u,DuDx)
global Q;
global H;
global W;
global D;
As=H*W;%cross-sectional area of the reactor
v=Q/As; %velocity
c=v/D;
f=DuDx;
s=0;
end
%% Initial conditions
function u0=pdeic(x)
global Cao;
u0=Cao;
end
%% Boundary conditions
function[pl,ql,pr,qr]=pdebc(xl,ul,xr,ur,t)
global E;
global alpha;
global th;
global KA;
global k;
global n;
Ea_avg=alpha*E/(alpha*th)*(1-exp(-alpha*th));
rA=-1*Ea_avg^n*k*KA.*ul./(1+KA.*ul); %reaction rate

pl=rA;
ql=1;
pr=0;
qr=1;
end
%   This model solves the material balance along the photoreactor
%   for different reactor heights
%   The equation to be solved is: -v*dCA/dx+D*d^2CA/dz^2=0
%   with the boundary conditions: at the top of the reactor dC/dz=0
%   and at the bottom the reaction: D*dC/dz=-rA (the reaction takes
place)
%   The pdepe solver can solve equations of the form:
%   c(x,t,y,du/dx)*du/dt=x^-m*d/dx(d^m f(x,t,u,du/dx)) +
s(x,t,u,du/dx)
%   Let c=v/D, t->x, x->z, u->C
 function Photoreactor_diff_heights
    clear
    clc
 %% Photoreactor dimensions
 %Flow rate
 global Q
 t=10; %hours
```

```
 Flow=0.05;%m3/day
 Q=Flow/(t*3600);%m3/s
 %Photoreactor heights
 global z1
 z1=0.001;
 global z2
 z2=0.002;
 global z3
 z3=0.003;
 global z4
 z4=0.005;
 global z5
 z5=0.01;
 %Photoreactor dimensions
 global H
 H=60;%m
 global W
 W=0.4;%m
 %% Physicochemical properties
 global CAo
 CAo=1; %initial concentration
 global k
 k=0.5226e-3; % reaction constant
 global D
 D=9.1e-10; %diffusion coefficient [m2/s]
 global E %Irradiation W/m2
 E=25;
 global n %reaction order with respect to the light absorption
 n=1;
 global KA %equilibrium adsorption constant
 KA=0.85;
%% Solution
m=0; %(cartesian coordinates)
zmesh_z1=linspace(0,z1,500);
zmesh_z2=linspace(0,z2,500);
zmesh_z3=linspace(0,z3,500);
zmesh_z4=linspace(0,z4,500);
zmesh_z5=linspace(0,z5,500);
xspan=linspace(0,H,500);

sol_z1=pdepe(m,@pdefun_z1,@pdeic,@pdebc,zmesh_z1,xspan);
u_z1=sol_z1(:,:,1);
sol_z2=pdepe(m,@pdefun_z2,@pdeic,@pdebc,zmesh_z2,xspan);
u_z2=sol_z2(:,:,1);
sol_z3=pdepe(m,@pdefun_z3,@pdeic,@pdebc,zmesh_z3,xspan);
u_z3=sol_z3(:,:,1);
sol_z4=pdepe(m,@pdefun_z4,@pdeic,@pdebc,zmesh_z4,xspan);
u_z4=sol_z4(:,:,1);
sol_z5=pdepe(m,@pdefun_z5,@pdeic,@pdebc,zmesh_z5,xspan);
u_z5=sol_z5(:,:,1);
    subplot(1,2,1)
    plot(xspan(end,:),u_z1(:,end))
    hold on
    plot(xspan(end,:),u_z2(:,end))
    hold on
    plot(xspan(end,:),u_z3(:,end))
    hold on
    plot(xspan(end,:),u_z4(:,end))
    hold on
    plot(xspan(end,:),u_z5(:,end))
```

```
    %title('Conversion profile at different heights')
    title('(a)')
    xlabel('Photoreactor length [m]')
    ylabel('Pollutant conversion [-]')
    legend('Z=0.1cm','Z=0.2cm','Z=0.3cm', 'Z=0.5cm', 'Z=1cm')

    %Computing the residence time
    %Finding the length of the reactor to reach 95% conversion
X_point=xspan(end,:);
Y_point_uz1 = u_z1(:,end);
Y_point_uz2 = u_z2(:,end);
Y_point_uz3 = u_z3(:,end);
Y_point_uz4 = u_z4(:,end);
%     Y_point_uz5 = u_z5(:,end);
xDesired_uz1 = interp1(Y_point_uz1,X_point,0.05);
xDesired_uz2 = interp1(Y_point_uz2,X_point,0.05);
xDesired_uz3 = interp1(Y_point_uz3,X_point,0.05);
xDesired_uz4 = interp1(Y_point_uz4,X_point,0.05);
%      xDesired_uz5 = interp1(Y_point_uz5,X_point,0.05,'cubic');

v_z1=Q/(W*z1);
v_z2=Q/(W*z2);
v_z3=Q/(W*z3);
v_z4=Q/(W*z4);

tao_uz1=xDesired_uz1/(v_z1*3600);
tao_uz2=xDesired_uz2/(v_z2*3600);
tao_uz3=xDesired_uz3/(v_z3*3600);
tao_uz4=xDesired_uz4/(v_z4*3600);
tao=[tao_uz1 tao_uz2 tao_uz3 tao_uz4];
z=[z1 z2 z3 z4];
    subplot(1,2,2)
    plot(z.*100,tao,'--*')
    xlabel('Photoreactor height [cm]')
    ylabel('Residence time [h]')
    title('(b)')
 end
 %% Function to be solved
function[c,f,s]=pdefun_z1(x,t,u,DuDx)
global z1;
global Q;
global D;
global W;
As=z1*W;%cross-sectional area of the reactor.
v=Q/As; %velocity
c=v/D;
f=DuDx;
s=0;
end
function[c,f,s]=pdefun_z2(x,t,u,DuDx)
global z2;
global Q;
global D;
global W;
As=z2*W;%cross-sectional area of the reactor
v=Q/As; %velocity
c=v/D;
f=DuDx;
s=0;
end
function[c,f,s]=pdefun_z3(x,t,u,DuDx)
```

```
global z3;
global Q;
global D;
global W;
As=z3*W;%cross-sectional area of the reactor
v=Q/As; %velocity
c=v/D;
f=DuDx;
s=0;
end
function[c,f,s]=pdefun_z4(x,t,u,DuDx)
global z4;
global Q;
global D;
global W;
As=z4*W;%cross-sectional area of the reactor
v=Q/As; %velocity
c=v/D;
f=DuDx;
s=0;
end
function[c,f,s]=pdefun_z5(x,t,u,DuDx)
global z5;
global Q;
global D;
global W;
As=z5*W;%cross-sectional area of the reactor.
v=Q/As;
D=9.1e-10;
c=v/D;
f=DuDx;
s=0;
end
%% Initial conditions
function u0=pdeic(x)
global CAo;
u0=CAo;
end
%% Boundary conditions
function[pl,ql,pr,qr]=pdebc(xl,ul,xr,ur,t)
global E;
global n;
global k;
global KA;
th=4e-6;%catalytic film thickness [m]
alpha=1.02e6;%[m-1] Extinction coefficient film
Ea_avg=alpha*E/(alpha*th)*(1-exp(-alpha*th));
rA=-1*Ea_avg^n*k*KA.*ul./(1+KA.*ul); %reaction rate
pl=rA;
ql=1;
pr=0;
qr=1;
end
%   This model computes the comparison between the diffusion and
reaction rates of
%   the pollutant degradation at the top zone of the photoreactor
%   The equation to be solved is: -v*dC/dx+D*d^2C/dz^2=0
%   with the boundary conditions: at the top of the reactor dC/dz=0
%   and at the bottom the reaction: D*dC/dz=-rA (the reaction takes
place)
function model_photoreactor_length_diffD_R
```

```
clear
clc
%% Reactor dimensions
global H; %height of the reactor
H=0.01; %m
global L; %length of the reactor
L=60;%m
global W;%width of the reactor
W=0.4;%m
Water=0.05;%flow in m3 per day
t_sun=10;%assuming 10 hours of sun per day
global Q;
Q=Water/(t_sun*3600); %m3/s of water to be treated
%% Physicochemical properties
global D;
D=9.1e-10; %diffusion coefficient [m2/s]
global Cao;
Cao=1; %mol/m3
global th;
th=4e-6;%catalytic film thickness [m]
global alpha;
alpha=1.02e6;%[m-1] Extinction coefficient film
global E;
E=25;% Intensity W/m2
global n;
n=1; %reaction order with respect to the light absorption
global k;
k=0.5226e-3; % reaction constant molm^2/m^2sW
global KA;
KA=0.85;% adsorption contant m3/mol
%% Solution
m=0; %for the flat plate (cartesian coordinates)
zmesh=linspace(0,H,200); %thickness of the photoreactor [m]
xspan=linspace(0,L,200); %length of the photoreactor [m]
%Initial conditions
sol=pdepe(m,@pdefun,@pdeic,@pdebc,zmesh,xspan);
u=sol(:,:,1);
%Faster reaction rate
sol1=pdepe(m,@pdefun,@pdeic,@pdebc1,zmesh,xspan);
u1=sol1(:,:,1);
%Slower reaction rate
sol2=pdepe(m,@pdefun,@pdeic,@pdebc2,zmesh,xspan);
u2=sol2(:,:,1);
%Higher diffusion coefficient
sol3=pdepe(m,@pdefun3,@pdeic,@pdebc3,zmesh,xspan);
u3=sol3(:,:,1);
%Lower diffusion coefficient
sol4=pdepe(m,@pdefun4,@pdeic,@pdebc4,zmesh,xspan); %Diffusion 2 times
slower
u4=sol4(:,:,1); %Diffusion 2x slower

subplot(1,2,1) %Effect of the reaction rate
    plot(xspan(end,:),u2(:,end))
    hold on
    plot(xspan(end,:),u(:,end))
    hold on
    plot(xspan(end,:),u1(:,end))
    %title('Conversion profile at different depths')
    xlabel('Photoreactor length [m]')
    ylabel('Pollutant conversion [-]')
    legend( '-1/2r_{A}','-r_{A}', '-2r_{A}')
```

```
    title('(a)')
subplot(1,2,2) %effect of the diffusion
    plot(xspan(end,:),u4(:,end))
    hold on
    plot(xspan(end,:),u(:,end))
    hold on
    plot(xspan(end,:),u3(:,end))
    %title('Conversion profile at different depths')
    xlabel('Photoreactor length [m]')
    ylabel('Pollutant conversion [-]')
    legend('1/2D','D', '2D')
    title('(b)')
end
%% function to be solved
function[c,f,s]=pdefun(x,t,u,DuDx)
global Q;
global H;
global W;
global D;
As=H*W;%cross-sectional area of the reactor
v=Q/As; %velocity
c=v/D;
f=DuDx;
s=0;
end
%% Initial conditions
function u0=pdeic(x)
global Cao;
u0=Cao;
end
%% Boundary conditions
% Base case scenario
function[pl,ql,pr,qr]=pdebc(xl,ul,xr,ur,t)
global E;
global alpha;
global th;
global KA;
global k;
global n;
Ea_avg=alpha*E/(alpha*th)*(1-exp(-alpha*th));
rA=-1*Ea_avg^n*k*KA.*ul./(1+KA.*ul); %reaction rate

pl=rA;
ql=1;
pr=0;
qr=1;
end
% Faster reaction rate
function[pl,ql,pr,qr]=pdebc1(xl,ul,xr,ur,t)
global E;
global alpha;
global th;
global KA;
global k;
global n;
Ea_avg=alpha*E/(alpha*th)*(1-exp(-alpha*th));
rA=-2*Ea_avg^n*k*KA.*ul./(1+KA.*ul); %reaction rate

pl=rA;
ql=1;
pr=0;
```

```
qr=1;
end
% Slower reaction rate
function[pl,ql,pr,qr]=pdebc2(xl,ul,xr,ur,t)
global E;
global alpha;
global th;
global KA;
global k;
global n;
Ea_avg=alpha*E/(alpha*th)*(1-exp(-alpha*th));
rA=-1/2*Ea_avg^n*k*KA.*ul./(1+KA.*ul); %reaction rate

pl=rA;
ql=1;
pr=0;
qr=1;
end
% Higher diffusion coefficient
function[c,f,s]=pdefun3(x,t,u,DuDx)
global Q;
global H;
global W;
global D;
De=2*D;
As=H*W;%cross-sectional area of the reactor
v=Q/As; %velocity
c=v/De;
f=DuDx;
s=0;
end
function[pl,ql,pr,qr]=pdebc3(xl,ul,xr,ur,t)
global E;
global alpha;
global th;
global KA;
global k;
global n;
Ea_avg=alpha*E/(alpha*th)*(1-exp(-alpha*th));
rA=-1*Ea_avg^n*k*KA.*ul./(1+KA.*ul); %reaction rate

pl=rA;
ql=1;
pr=0;
qr=1;
end
% Lower diffusion coefficient
function[c,f,s]=pdefun4(x,t,u,DuDx)
global Q;
global H;
global W;
global D;
De=0.5*D;
As=H*W;%cross-sectional area of the reactor
v=Q/As; %velocity
c=v/De;
f=DuDx;
s=0;
end
function[pl,ql,pr,qr]=pdebc4(xl,ul,xr,ur,t)
global E;
```

```
global alpha;
global th;
global KA;
global k;
global n;
Ea_avg=alpha*E/(alpha*th)*(1-exp(-alpha*th));
rA=-1*Ea_avg^n*k*KA.*ul./(1+KA.*ul); %reaction rate

pl=rA;
ql=1;
pr=0;
qr=1;
end
```

Appendix C: Photocatalyst modelling

```
function slab_photoreactor_concentration
clear
clc
global n;
n=1;
global E;
E=25;
global k;
k=0.5226e-3; %kinetic constant [mol*m^2/(m^2*s*W)]
global K;
K=0.85; %adsorption constant [m3/mol]
global De;
De=2.929e-10; %diffusion coefficient [m2/s]
global CAs;
CAs=1;

solinit=bvpinit(0:0.0001:1,[1,1]);
%Concentration at different catalyst thickness
sol=bvp4c(@base,@bcs,solinit);
sol2th=bvp4c(@thickness2,@bcs,solinit);
sol5th=bvp4c(@thickness5,@bcs,solinit);
subplot(2,2,1)
plot(sol2th.x,sol2th.y(1,:));
hold on
plot(sol.x,sol.y(1,:));
hold on
plot(sol5th.x,sol5th.y(1,:));
legend('l_{gs}=3\mum','l_{gs}=4\mum','l_{gs}=5\mum')
xlabel('$\bar{\sigma}$ [-]','Interpreter','latex')
ylabel('$\bar{c}$ [-]','Interpreter','latex')
title('(a)')
%different eq adsorption constants
sol02ads=bvp4c(@ads02,@bcs,solinit);
sol05ads=bvp4c(@ads05,@bcs,solinit);
sol2ads=bvp4c(@ads2,@bcs,solinit);
sol3ads=bvp4c(@ads3,@bcs,solinit);
subplot(2,2,2)
plot(sol02ads.x,sol02ads.y(1,:));
hold on
plot(sol05ads.x,sol05ads.y(1,:));
hold on
plot(sol.x,sol.y(1,:));
hold on
plot(sol2ads.x,sol2ads.y(1,:));
hold on
plot(sol3ads.x,sol3ads.y(1,:));
legend('0.2\phi_{0}','0.5\phi_{0}','\phi_{0}','2\phi_{0}','3\phi_{0}'
)
xlabel('$\bar{\sigma}$ [-]','Interpreter','latex')
ylabel('$\bar{c}$ [-]','Interpreter','latex')
title('(b)')
%different thiele modulus
soltm05=bvp4c(@tm05,@bcs,solinit);
soltm2=bvp4c(@tm2,@bcs,solinit);
soltm3=bvp4c(@tm3,@bcs,solinit);
subplot(2,2,3.5)
plot(soltm05.x,soltm05.y(1,:));
hold on
```

```
plot(sol.x,sol.y(1,:));
hold on
plot(soltm2.x,soltm2.y(1,:));
hold on
plot(soltm3.x,soltm3.y(1,:));
legend('0.5\Theta_{0}','\Theta_{0}','2\Theta_{0}','3\Theta_{0}')
xlabel('$\bar{\sigma}$ [-]','Interpreter','latex')
ylabel('$\bar{c}$ [-]','Interpreter','latex')
title('(c)')

end

function dydx=base(x,y)
global CAs;
global De;
global k;
global E;
global K;
global n;

a=4e-6; %film thickness [m]
alpha=1.0222;%um-1 Extinction coefficient film
alpha_=1.0222e6;%m-1 ectinction coefficient for ea
th=4;%um

Ea=alpha_*E/(alpha*th)*(1-exp(-alpha*th));
Theta=K*CAs;
Gamma=Theta./(Theta+1).*((k*K*a^2.*(Ea).^n)./(2*De*(Theta-
log(1+Theta)))).^0.5;
dydx(1)=y(2);
dydx(2)=Gamma.^2.*y(1)./(1+Theta.*y(1));
end

%% Effect of different photocatalytic thickness
function dydx=thickness2(x,y)
global CAs;
global De;
global k;
global E;
global K;
global n;
a=3e-6; %film thickness [m]
alpha=1.0222;%um-1 Extinction coefficient film
alpha_=1.0222e6;%m-1 ectinction coefficient for ea
th=3;%um
Ea=alpha_*E/(alpha*th)*(1-exp(-alpha*th));

Theta=K*CAs;
Gamma=Theta./(Theta+1).*((k*K*a^2.*(Ea).^n)./(2*De*(Theta-
log(1+Theta)))).^0.5;
dydx(1)=y(2);
dydx(2)=Gamma.^2.*y(1)./(1+Theta.*y(1));
end
function dydx=thickness5(x,y)
global CAs;
global De;
global k;
global E;
global K;
global n;
a=5e-6; %film thickness [m]
```

```
alpha=1.0222;%um-1 Extinction coefficient film
alpha_=1.0222e6;%m-1 ectinction coefficient for ea
th=5;%um

Ea=alpha_*E/(alpha*th)*(1-exp(-alpha*th));

Theta=K*CAs;
Gamma=Theta./(Theta+1).*((k*K*a^2.*(Ea).^n)./(2*De*(Theta-
log(1+Theta)))).^0.5;
dydx(1)=y(2);
dydx(2)=Gamma.^2.*y(1)./(1+Theta.*y(1));
end
%% Effect of the equilibrium adsorption constant
function dydx=ads02(x,y)
global CAs;
global De;
global k;
global E;
global K;
global n;

KA=0.2*K; %adsorption constant [m3/mol]
a=4e-6; %film thickness [m]
alpha=1.0222;%um-1 Extinction coefficient film
alpha_=1.0222e6;%m-1 ectinction coefficient for ea
th=4;%um
Ea=alpha_*E/(alpha*th)*(1-exp(-alpha*th));

Theta=KA*CAs;
Gamma=Theta./(Theta+1).*((k*KA*a^2.*(Ea).^n)./(2*De*(Theta-
log(1+Theta)))).^0.5;
dydx(1)=y(2);
dydx(2)=Gamma.^2.*y(1)./(1+Theta.*y(1));
end
function dydx=ads05(x,y)
global CAs;
global De;
global k;
global E;
global K;
global n;

KA=0.5*K; %adsorption constant [m3/mol]
a=4e-6; %film thickness [m]
alpha=1.0222;%um-1 Extinction coefficient film
alpha_=1.0222e6;%m-1 ectinction coefficient for ea
th=4;%um
Ea=alpha_*E/(alpha*th)*(1-exp(-alpha*th));

Theta=KA*CAs;
Gamma=Theta./(Theta+1).*((k*KA*a^2.*(Ea).^n)./(2*De*(Theta-
log(1+Theta)))).^0.5;
dydx(1)=y(2);
dydx(2)=Gamma.^2.*y(1)./(1+Theta.*y(1));
end
function dydx=ads2(x,y)
global CAs;
global De;
global k;
global E;
global K;
```

```
global n;
KA=2*K; %adsorption constant [m3/mol]
a=4e-6; %film thickness [m]
alpha=1.0222;%um-1 Extinction coefficient film
alpha_=1.0222e6;%m-1 ectinction coefficient for ea
th=4;%um
Ea=alpha_*E/(alpha*th)*(1-exp(-alpha*th));

Theta=KA*CAs;
Gamma=Theta./(Theta+1).*((k*KA*a^2.*(Ea).^n)./(2*De*(Theta-
log(1+Theta)))).^0.5;
dydx(1)=y(2);
dydx(2)=Gamma.^2.*y(1)./(1+Theta.*y(1));
end
function dydx=ads3(x,y)
global CAs;
global De;
global k;
global E;
global K;
global n;

KA=3*K; %adsorption constant [m3/mol]
a=4e-6; %film thickness [m]
alpha=1.0222;%um-1 Extinction coefficient film
alpha_=1.0222e6;%m-1 ectinction coefficient for ea
th=4;%um
Ea=alpha_*E/(alpha*th)*(1-exp(-alpha*th));

Theta=K*CAs;
Gamma=Theta./(Theta+1).*((k*K*a^2.*(Ea).^n)./(2*De*(Theta-
log(1+Theta)))).^0.5;
dydx(1)=y(2);
dydx(2)=Gamma.^2.*y(1)./(1+Theta.*y(1));
end
%% Effect of the thiele modulus
function dydx=tm05(x,y)
global CAs;
global De;
global k;
global E;
global K;
global n;

a=4e-6; %film thickness [m]
alpha=1.0222;%um-1 Extinction coefficient film
alpha_=1.0222e6;%m-1 ectinction coefficient for ea
th=4;%um
Ea=alpha_*E/(alpha*th)*(1-exp(-alpha*th));

Theta=K*CAs;
Gamma=0.5*Theta./(Theta+1).*((k*K*a^2.*(Ea).^n)./(2*De*(Theta-
log(1+Theta)))).^0.5;
dydx(1)=y(2);
dydx(2)=Gamma.^2.*y(1)./(1+Theta.*y(1));
end
function dydx=tm2(x,y)
global CAs;
global De;
global k;
global E;
```

```
global K;
global n;
a=4e-6; %film thickness [m]

alpha=1.0222;%um-1 Extinction coefficient film
alpha_=1.0222e6;%m-1 ectinction coefficient for ea
th=4;%um
Ea=alpha_*E/(alpha*th)*(1-exp(-alpha*th));

Theta=K*CAs;
Gamma=2*Theta./(Theta+1).*((k*K*a^2.*(Ea).^n)./(2*De*(Theta-
log(1+Theta)))).^0.5;
dydx(1)=y(2);
dydx(2)=Gamma.^2.*y(1)./(1+Theta.*y(1));
end
function dydx=tm3(x,y)
global CAs;
global De;
global k;
global E;
global K;
global n;
a=4e-6; %film thickness [m]
alpha=1.0222;%um-1 Extinction coefficient film
alpha_=1.0222e6;%m-1 ectinction coefficient for ea
th=4;%um
Ea=alpha_*E/(alpha*th)*(1-exp(-alpha*th));

Theta=K*CAs;
Gamma=3*Theta./(Theta+1).*((k*K*a^2.*(Ea).^n)./(2*De*(Theta-
log(1+Theta)))).^0.5;
dydx(1)=y(2);
dydx(2)=Gamma.^2.*y(1)./(1+Theta.*y(1));
end
%% Boundary conditions
%boundary conditions y'(a)=0, y(b)=1 (a,b)=(0,1)
function res=bcs(ya,yb)
res=[ya(1)-1;yb(2)];
end
```